Powder Technology 467 (2026) 121507

Contents lists available at ScienceDirect

Powder Technology

journal homepage: www.journals.elsevier.com/powder-technology

An adaptive and bi-directional PBM-DEM framework for multi-component wet granulation: Bridging the gap between computational efficiency and High-fidelity model physics

Tarun De [a], Ashley Dan [b], Rohit Ramachandran [b], Ashok Das [c,*]

[a] Department of Chemical Engineering, Indian Institute of Technology Kanpur, Uttar Pradesh 208016, India
[b] Department of Chemical and Biochemical Engineering, Rutgers, The State University of New Jersey, Piscataway, NJ 08854, USA
[c] Department of Mathematics and Computing, Indian Institute of Technology (ISM) Dhanbad, Jharkhand 826004, India

HIGHLIGHTS

- Efficient PBM growth model from liquid addition validated using DEM simulations.
- Adaptive system scaling in DEM to reduce computational cost with fixed particle count.
- The above components implemented in 3D bi-directional PBM-DEM framework. successfully
- Wet granulation size and composition predicted under varying liquid rates and ratios.

GRAPHICAL ABSTRACT

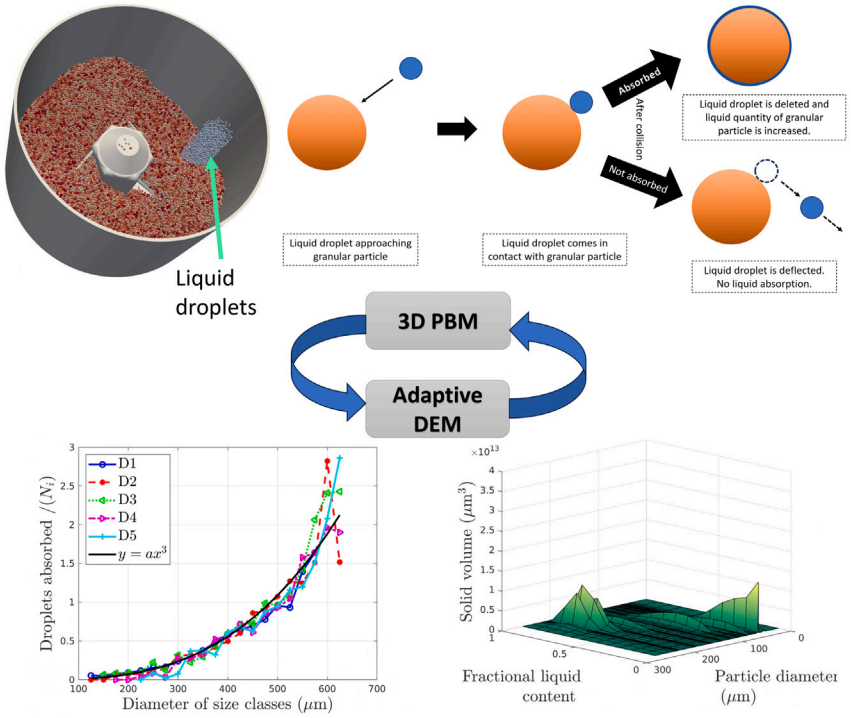

ARTICLE INFO

Keywords:
Multi-dimensional PBM
Adaptive DEM geometry
Liquid addition

ABSTRACT

This study introduces a novel bi-directional and bi-component coupling framework that integrates Population Balance Modeling (PBM) and the Discrete Element Method (DEM) for simulating wet granulation processes. In conventional approaches, we have treated liquid droplets as granular particles in DEM, which has led

* Corresponding author.
E-mail address: ashokdas@iitism.ac.in (A. Das).

https://doi.org/10.1016/j.powtec.2025.121507
Received 21 May 2025; Received in revised form 24 July 2025; Accepted 31 July 2025
Available online 13 August 2025

DEM-PBM coupling
Granulation

to significant computational demands due to the generation and deletion of liquid droplets. To address this challenge, we establish a relationship between granule size and their liquid absorption rate utilizing DEM. Consequently, we propose a novel mechanistic formulation that incorporates liquid droplets within the PBM, enhancing the framework's ability to accurately simulate particle-liquid interactions, which are crucial for granulation outcomes. Additionally, we introduce an adaptive system scaling method (ASSM) within DEM that dynamically adjusts system dimensions to accommodate a fixed number of particles, reducing computational resources by 82% while maintaining simulation accuracy. We have further validated the proposed framework against experimental data. Moreover, integrating these advancements, we investigated the effects of key process parameters, such as liquid-to-solid ratio and liquid addition duration, on granulation processes. Results indicate a computational cost saving of fivefold through the implementation of ASSM.

1. Introduction

Wet granulation plays an important role in various industries, with a particular emphasis on pharmaceuticals, where it serves to enhance the properties of powder blends. The process entails the amalgamation of powder particles with a liquid binder to create aggregates, resulting in improved powder flowability, compressibility, and uniformity, which are attributes critical for the production of tablets and capsules. In the pharmaceutical sector, wet granulation is indispensable for ensuring consistent drug dosage, stability, and a reduction in dust, thereby contributing to a safer and cleaner production environment. Its versatility extends beyond pharmaceuticals, finding applications in food, agriculture, detergents, and chemicals. Bi-component wet granulation [1], a more complex technique than the single-component process, introduces a second solid component during the granulation process. This provides enhanced control over granule functionality such as control of dissolution rates. In pharmaceutical applications, the bi-component formulation involves combining an active pharmaceutical ingredient (API) with excipients, enabling precise drug release and stability. Notably, this method facilitates the production of different solid dosage forms for both immediate and sustained release profiles. Such innovation can potentially enhance medication efficacy and supports the development of cutting-edge drug delivery systems, to enhance alignment with evolving healthcare and pharmaceutical requirements [2]. The existing literature offers an array of methods for modeling these particulate processes, such as population balance models [3,4], discrete element methods [5,6], computational fluid dynamics [7,8], and the Monte Carlo techniques [9].

The population balance method (PBM) and discrete element method (DEM) are prominent modeling techniques for granulation processes, each with distinct advantages and limitations. PBM employs integro-differential population balance equations (PBEs) to monitor particle characteristics influenced by rate mechanisms such as nucleation, growth, and aggregation [10]. While analytical solutions exist for simplified cases [11], most scenarios require advanced numerical methods, including finite element [12], finite volume [3,4], cell average [13], and moment [14] methods, ensuring computational efficiency critical for industries like pharmaceuticals [15]. However, PBM relies on empirical kernels, which may lead to mismatches with experimental results [16,17] and neglects particle-level nuances crucial for specialized applications. In contrast, DEM simulates individual particles using Newton's laws, offering detailed insights into granular system. Although originally applied to rock mechanics [18], DEM has moved into other disciplines such as biomaterials [19], manufacturing [20], powder technology [21], etc. The first models in two dimensions employed circular [5] and polygonal [22] particles, which were later advanced by spherical [23], triangulated [6] and superquadric [24] particles in three dimensions. Although the non-spherical shape of particles brings a more realistic approach to the granulation process, we confine our work to spherical shape for ease of modeling. Even if researchers use a very simplistic particle model, only smaller subdomains, and almost stationary solutions, the DEM [5] solution remains computationally infeasible for industrial systems. While DEM captures temporal particle dynamics, DEM struggles with computational challenges in aggregation and breakage, limiting its efficiency for large-scale applications [21]. Despite these challenges, both methods complement each other in addressing granulation complexities.

Despite challenges, DEM has been successfully applied to model granulation with particle breakage, predicting key process dynamics in some studies [25]. However, its application to particle aggregation remains underexplored, highlighting a gap in current capabilities. DEM's detailed approach is valuable for granular processes but is computationally demanding, particularly for industrial systems involving fragmentation and aggregation. To address this, coupling PBM and DEM has gained interest due to their complementary strengths. PBM predicts macroscopic outcomes but lacks integration of system attributes, while DEM tracks particle-level dynamics, providing microscale data (e.g., collision frequency, forces) for refining PBM kernels. This coupling approach has been explored for univariate systems, with initial studies focusing on one-way coupling for formulating aggregation and breakage kernels [26,27]. Recent works [1,15,28–30] improved bi-directional PBM-DEM coupling by prioritizing PBM, introducing advanced collision detection, and coarse-graining techniques, enhancing accuracy and efficiency. However, a significant gap persists in multi-dimensional PBM-DEM frameworks with improved mechanistic descriptions for accurately simulating multi-component granule dynamics.

In this study, we propose a new bi-directional three-dimensional PBM-DEM coupling framework in the presence of liquid droplets, aiming to achieve greater accuracy and efficiency in modeling bi-component granulation processes. The proposed model is developed to improve the efficiency of the PBM-DEM coupling by integrating liquid addition mechanism directly into the PBM through the introduction of a new mathematical formulation for improved computational efficiency. To further enhance efficiency and facilitate the simulation of industrial-scale systems, a novel adaptive DEM system scaling approach is introduced for the first time in the literature.

The structure of this article is organized as follows: Section 2 provides an overview of the DEM, PBM, and introduces the proposed bi-directional and bi-component PBM-DEM coupling framework. Section 3 focuses on verifying the proposed mathematical models of liquid addition and system scaling approaches. The verification process is conducted for several system specifications to discuss its generalized applicability. The predictions and new results of the proposed multi-component bi-directional PBM-DEM simulation for different test cases are presented in Section 4. Finally, Section 5 consolidates the key insights and conclusions drawn from the research.

2. Description of simulation framework

This section offers an in-depth description of the multi-dimensional PBM, DEM, and their proposed bi-directional coupling technique. The primary objective is to observe the evolution of the size and component distributions of bi-component (solid) particles within a granulator under continuous liquid flow. Key properties considered in our analysis include the volume, chemical content, and liquid absorption rate of the particles. The word "dimension" refers to the internal properties of particles, not their spatial properties.

List of Abbreviations and Notations

Nomenclature

α, δ	Adjustable parameters in aggregation kernel
β	Aggregation kernel
β_0	Aggregation rate coefficient
Δt_{sim}	Simulation process time interval
Δt_C	Rayleigh critical time step
Δt_{DEM}	DEM time step
Δt_{DEM}	Simulation time step
δ_{nor}	Normal overlap between particles
δ_{tang}	Tangential displacement
$\dot{N}_w$	Number inflow rate of binder droplets
$\gamma_{\text{nor}}, \gamma_{\text{tang}}$	Damping constants (normal, tangential)
$\kappa_{\text{nor}}, \kappa_{\text{tang}}$	Elastic constants (normal, tangential)
μ_r	Coefficient of rolling friction
μ_r	Coefficient of rolling friction
μ_s	Coefficient of static friction
ν	Poisson's ratio
ν	Poisson's ratio
Φ	Proportionality constant for liquid absorption
ψ	Absorption percentage of a granule
ρ	Density
θ	One-third of mean square velocity
$\vec{\omega}_i$	Angular velocity of particle i
$\vec{F}_i^{\text{ext}}$	External force on particle i
$\vec{F}_{\text{nor},ij}$	Normal contact force between i and j
$\vec{F}_{\text{tang},ij}$	Tangential contact force between i and j
$\vec{F}_{c,ij}$	Contact force between particles i and j
$\vec{v}_i$	Velocity vector of particle i
$\vec{x}_i$	Position vector of particle i
AC	API content fraction, $AC = \frac{s_1}{s_1+s_2}$
d_p	Particle diameter
E	Young's modulus (Pa)
E	Young's modulus
e	Coefficient of restitution
E^*	Effective modulus
f_c	Number-normalized collision frequency
$f_{\text{c,tot}}$	Total collision frequency per unit volume
G	Shear modulus
G^*	Effective shear modulus
g_0	Radial distribution function
G_{liq}	Volumetric growth rate of liquid in granules
I_i	Moment of inertia of particle i
l_i	Coarse-graining ratio at iteration i
LC	Liquid content fraction, $LC = \frac{l}{s_1+s_2+w}$
m^*	Effective mass
m_i	Mass of particle i
N	Number of particles in a class
n	Number density function of granuless
N_p	Total number of particles
N_{coll}	Number of collisions between two particle classes
N_{orig}	Original (resolved) number of particle
N_{scaled}	Scaled (coarse-grained) number of particles
R^*	Effective radius
r_0	Initial average particle radius
r_i	Average particle radius at iteration i
s_1	Volume of API in a granule
s_2	Volume of excipient in a granule
SC	Solid content fraction, $SC = \frac{s_1+s_2}{s_1+s_2+w}$
V	Gross volume of a granule, $V = s_1 + s_2 + w$
w	Volume of binder liquid in a granule
API	Active Pharmaceutical Ingredient
ASSM	Adaptive System Scaling Method
CG	Coarse-Grained
DEM	Discrete Element Method
EXP	Excipient
LS	Liquid-to-solid ratio
PBE	Population Balance Equation
PBM	Population Balance Model
PSD	Particle Size Distribution
RPM	Revolutions per minute (impeller speed)

2.1. Multi-dimensional population balance model

PBM serves to describe the behavior of discrete entities in response to time-dependent influences. It explains alterations in the number densities of distinct particle types within a granulator, influenced by influential granulation mechanisms, such as particle growth resulting from liquid addition and aggregation due to particle interactions. During granulation, if we consider the composition and particle volume to be the most crucial granule characteristics, a three-dimensional PBM is sufficient to describe the physics of the process. For this, we employ the following three-dimensional PBE:

$$\frac{\partial n(s_1,s_2,w,t)}{\partial t} + \frac{\partial}{\partial w}[G_{liq}(s_1,s_2,w,t)\, n(s_1,s_2,w,t)] = \frac{1}{2}\int_0^{s_1}\int_0^{s_2}\int_0^{w} \beta(x,y,z;s_1-x,s_2-y,w-z;t)\, n(s_1-x,s_2-y,w-z,t)\, n(x,y,z,t)\,\mathrm{d}x\,\mathrm{d}y\,\mathrm{d}z - \int_0^{\infty}\int_0^{\infty}\int_0^{\infty} \beta(x,y,z;s_1,s_2,w;t)\, n(s_1,s_2,w,t)\, n(x,y,z,t)\,\mathrm{d}x\,\mathrm{d}y\,\mathrm{d}z \quad (1)$$

along with the initial condition

$$n(s_1,s_2,w,0) = n_0(s_1,s_2,w), \qquad \text{for } (s_1,s_2,w) \in (\mathbb{R}^+)^3. \quad (2)$$

The characteristics of a granule are represented by the state vector (s_1, s_2, w) at time t, where s_1, s_2, and w are the volumes of API, excipient, and liquid, respectively. Total volume of the granule is the sum $s_1 + s_2 + w$, and total solid volume is $s_1 + s_2$. Solid, liquid, and API contents of the granule can be defined using the following equations:

$$SC = \frac{s_1+s_2}{s_1+s_2+w},\ LC = \frac{w}{s_1+s_2+w},\ AC = \frac{s_1}{s_1+s_2}. \quad (3)$$

Function $n(s_1, s_2, w, t)$ denotes the number density of granules comprising solid API volume (s_1), solid excipient volume (s_2), and binder liquid volume (w) at time t. $G_{liq}(s_1, s_2, w, t)$ represents the volumetric growth rate of liquid content in granules due to liquid addition mechanism. Formulation of this growth rate G_{liq} may vary depending on several factors, including liquid addition rate, particle size, and liquid absorption rate of different chemical components. A new mathematical

formulation of this particle growth rate is proposed later in this subsection and further verified with DEM simulations in the results and discussion Section 3 of this manuscript.

The PBE (1) includes terms for the birth and death rates of granules through aggregation, with the aggregation kernel $\beta(s_1, s_2, w; s_1', s_2', w'; t)$. This aggregation kernel indicates the number normalized rate of successful aggregation events during particle collisions. This kernel is symmetric in its first two coordinate sets, leading to a factor 1/2 in the first term on the right-hand side of the PBE (1). Moreover, this term, referred to as the birth term, signifies the rate of inclusion of particles with characteristic volume (s_1, s_2, w) due to successful collisions between all possible combinations of particles with volume coordinates $(s_1 - x, s_2 - y, w - z)$ and (x, y, z), respectively. The last term, known as the death term, expresses the removal rate of particles from the class (s_1, s_2, w) due to collisional aggregation with other particles.

2.1.1. Aggregation kernel

For ensuring accurate prediction of results, it is crucial to model the aggregation kernel $\beta(s_1, s_2, w; s_1', s_2', w'; t)$. Numerous models and factorization techniques are available in the literature for the aggregation kernel [1,4,29,31,32]. One commonly adopted approach involves factorizing the aggregation kernel into size-independent and -dependant parts [29,31]. Another method is to decompose it into a collision frequency term between interacting particles and a collision efficiency term [1,32,33]. However, both of these approaches do not directly incorporate the effects of liquid content on the aggregation, despite it has been already established in the literature that final product granule size has a high dependence on the liquid-to-solid ratio parameter [34]. Madec et al. [35] developed a kernel capable of incorporating the effect of liquid content in addition to the particle volume parameter:

$$\beta_{Madec}(s_1, s_2, w; s_1', s_2', w'; t) = \beta_0 (V + V') \left[(LC + LC')^{\alpha} \left(1 - \frac{LC + LC'}{2} \right)^{\delta} \right]^{\alpha} \tag{4}$$

where V and V' represent the gross volume of the interacting particles, i.e., $(s_1 + s_2 + w)$ and $(s_1' + s_2' + w')$ respectively. This model encompasses three adjustable parameters: one aggregation rate coefficient β_0 and two exponential parameters α and δ, which represent the extent of liquid dependence. However, the Madec kernel assumes that every particle class can collide with all other particle classes including its own class, which often overestimates the aggregation term. Since collision frequency depends on particle characteristics and is critical for accurate aggregation modeling, the following modified aggregation kernel that simultaneously accounts for particle interactions and liquid content: is used:

$$\beta(s_1, s_2, w; s_1', s_2', w'; t) = f_c(s_1, s_2, w; s_1', s_2', w'; t) \times \left[\beta_0 (V + V') \left\{ (LC + LC')^{\alpha} \left(1 - \frac{LC + LC'}{2} \right)^{\delta} \right\}^{\alpha} \right] \tag{5}$$

where f_c denotes the number-normalized collision frequency between two particle size classes at instance t, which can be extracted from the DEM simulation as follows:

$$f_c(s_1, s_2, w; s_1', s_2', w'; t) = \frac{N_{coll}(s_1, s_2, w; s_1', s_2', w')}{N(s_1, s_2, w)\, N(s_1', s_2', w')\, \Delta t_{sim}} \tag{6}$$

where N_{coll} number of collisions occurring during the process time Δt_{sim} between particle classes (s_1, s_2, w) and (s_1', s_2', w'), containing $N(s_1, s_2, w)$ and $N(s_1', s_2', w')$ number of particles, respectively.

2.1.2. Liquid addition model

During wet granulation, binder liquid is introduced via sprayed droplets, which are absorbed by particles, increasing their liquid content and volume. This surface liquid, combined with impeller shear, promotes particle growth. Upon contact with solid particles, droplets either coat the surface or penetrate pores. The Madec aggregation kernel is more general in its description, considering both surface and absorbed liquid when calculating the liquid content. There are, however, aggregation kernels, such the semi-mechanistic kernel by Chaudhury et al. [36], that accounts specifically for the granule's fractional wetted area in the aggregation rate. Additionally, while these binder droplets can evaporate from the particle surfaces, this phenomenon falls outside the scope of this study. Accurate liquid deposition modeling is thus crucial for effectively predicting granulation.

One direct approach to calculating the volumetric growth rate from liquid addition involves conducting DEM simulations, recording liquid absorbed by each particle, and transferring this data to PBM calculations. However, storing and transferring liquid content for each particle across multiple DEM runs within the PBM-DEM framework is computationally expensive. Thus, efficient mathematical models are essential for an overall efficient coupling framework. While a few models exist [1,37], none of these models is physically accurate. In many cases, either equal distribution to each particle or an associated constant rate has been assumed by researchers [1]. However, the volumetric growth resulting from binder addition depends on factors like liquid flow rate, particle size, particle number, and absorption rate. To identify which size parameter correlates with this growth rate, several DEM simulations were conducted within this study, revealing that liquid addition rate on particle surface varies proportionally to particle volume. Section 3 details this verification.

Hence, the liquid droplets captured per unit time by a particle with volume vector (s_1, s_2, w) are proportional to $(s_1 + s_2 + w)\, n(s_1, s_2, w)\, \psi(s_1, s_2, w)$, where ψ denotes the absorption percentage of material. Summing over all particle classes yields:

$$\boldsymbol{\Phi} \int_0^{\infty} \int_0^{\infty} \int_0^{\infty} (s_1 + s_2 + w)\, n(s_1, s_2, w, t)\, \psi(s_1, s_2, w)\, \mathrm{d}s_1\, \mathrm{d}s_2\, \mathrm{d}w = \dot{N}_w \tag{7}$$

$$\Rightarrow \boldsymbol{\Phi} = \frac{\dot{N}_w}{\int_0^{\infty} \int_0^{\infty} \int_0^{\infty} (s_1 + s_2 + w)\, n((s_1, s_2, w, t))\, \psi(s_1, s_2, w)\, \mathrm{d}s_1\, \mathrm{d}s_2\, \mathrm{d}w} \tag{8}$$

where, $\dot{N}_w$ is the number inflow rate of the binder droplets, and $\boldsymbol{\Phi}$ is the proportionality constant. Finally the growth rate parameter in PBE (1) is

$$G_{liq}(s_1, s_2, w, t) = \boldsymbol{\Phi}\, (s_1 + s_2 + w)\, \psi(s_1, s_2, w). \tag{9}$$

2.2. Discrete element method

In DEM [5] simulations, each particle undergoes translational and rotational movements due to various forces and torques. These forces include body forces (e.g., gravity, electromagnetic forces), interactions with neighboring particles, and collisions with walls. The DEM tracks the motion of each particle using Newton's second law of motion. The governing equations for each particle are given as follows:

$$m_i \frac{\mathrm{d}\vec{v}_i}{\mathrm{d}t} = m_i \frac{\mathrm{d}^2 \vec{x}_i}{\mathrm{d}t^2} = \sum_{j=1}^{N_p} \vec{F}_{c,ij} + \vec{F}_i^{\mathrm{ext}}, \tag{10}$$

$$I_i \frac{\mathrm{d}\vec{\omega}_i}{\mathrm{d}t} = I_i \frac{\mathrm{d}^2 \vec{\theta}_i}{\mathrm{d}t^2} = \sum_{\substack{j=1 \\ j \neq i}}^{N_p} \vec{M}_{ij}^{t}. \tag{11}$$

N_p represents the total number of particles, m_i is the mass, $\vec{v}_i$ denotes the velocity, $\vec{x}_i$ represents the spatial position, I_i represents the moment of inertia, and $\vec{\omega}_i$ denotes the angular velocity of the ith particle. $\vec{F}_{c,ij}$, $\vec{F}_i^{\mathrm{ext}}$, and $\vec{M}_{ij}^{t}$ represent the contact force, external force, and tangential torque, respectively. External forces encompass both body forces and applied fields. The contact force $\vec{F}_{c,ij}$ includes both contact and long-range forces. In this study, DEM particles are considered dry due to the minimal and evenly distributed binder liquid on surfaces.

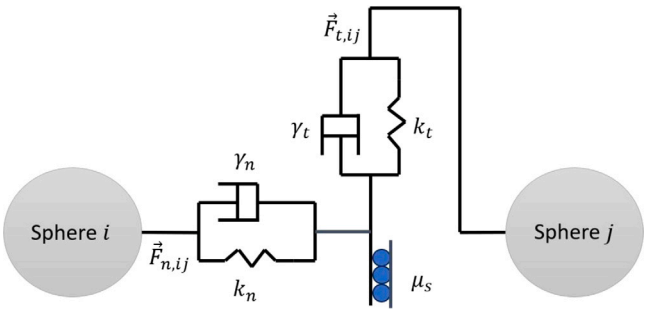

Fig. 1. Viscoelastic collision behavior depicted in the normal and tangential directions within the Hertz–Mindlin model.

Moreover, we adopt the Hertz–Mindlin contact model [30] to find the contact force between colliding particles. The contact forces ($\vec{F}_{c,i}$) acting on individual particles encompass both normal ($\vec{F}_{nor,ij}$) and tangential ($\vec{F}_{tang,ij}$) components. In the Hertz–Mindlin framework, the interaction between two approaching particles is conceptualized as a combination of a spring and a dashpot operating in parallel, as illustrated in Fig. 1. Consequently, the normal ($\vec{F}_{nor,ij}$) and tangential ($\vec{F}_{tang,ij}$) forces comprise elastic ($\vec{F}_{el}$) and dissipative ($\vec{F}_{diss}$) components. The Hertz–Mindlin model, which is a nonlinear viscoelastic model, provides accurate approximations for contact forces. The total contact force on a particle is expressed as:

$$\vec{F}_{c,i} = \vec{F}_{nor,ij} + \vec{F}_{tang,ij} = (\kappa_{nor}\vec{\delta}_{nor,ij} - \gamma_{nor}\vec{v}_{nor,ij}) + (\kappa_{tang}\vec{\delta}_{tang,ij} - \gamma_{tang}\vec{v}_{tang,ij}). \tag{12}$$

κ_{nor} and κ_{tang} denote the elastic constants, while γ_{nor} and γ_{tang} represent the damping constants along normal and tangential directions, respectively. The Hertz–Mindlin contact model equations are given by:

$$\begin{aligned} \kappa_{nor} &= \frac{4}{3}E^*\sqrt{R^*\delta_{nor}};\ \gamma_{nor} = -2\sqrt{\frac{5}{6}}\beta\sqrt{S_{nor}m^*}. \\ \kappa_{tang} &= 8G^*\sqrt{R^*\delta_{nor}};\ \gamma_{tang} = -2\sqrt{\frac{5}{6}}\beta\sqrt{S_{tang}m^*}. \\ S_{nor} &= 2Y^*\sqrt{R^*\delta_{nor}};\ S_{tang} = 8G^*\sqrt{R^*\delta_{nor}};\ \beta = \frac{\ln(e)}{\sqrt{(\ln(e))^2+\pi^2}}. \end{aligned} \tag{13}$$

The effective modulus, radius, shear modulus, mass, and restitution coefficient are represented by E^*, R^*, G^*, m^*, and e, respectively. DEM requires a simulation timestep smaller than the Rayleigh critical time (Δt_C) [15], which is calculated as:

$$\Delta t_C = \pi\left[\frac{R}{0.163\xi + 0.877}\sqrt{\frac{2\rho(1+\xi)}{E}}\right]. \tag{14}$$

The ξ and ρ denote the Poisson's ratio and density respectively. Ensuring accurate DEM simulation requires precise calibration of the timestep. In this study, we have maintained a DEM timestep (Δt_{DEM}) at 15% of Δt_C for all DEM simulations to uphold simulation accuracy.

Detection of collisions among particles is another time-consuming process in DEM, involving pairwise interactions between particles. Here, DEM simulations are primarily utilized for generating collision data among different particle classes. While various techniques exist in the literature [1,38] for storing DEM collision data, we adopt the recent approach proposed by Das et al. [15]. This approach by Das et al. [15] efficiently calculates collision data while maintaining accuracy in calculation. This method avoids repeated collision calculations in subsequent time steps by comparing the current neighbor list of particles with the previous one. In DEM simulations, the time step (Δt_{DEM}) is typically very small, and in densely packed systems, particles remain in contact during collisions for durations exceeding Δt_{DEM}. To enhance efficiency, the particle neighbor list is compared at intervals of several DEM time steps rather than at every Δt_{DEM}. The authors demonstrated that using a collision detection interval of $50\,\Delta t_{DEM}$, instead of Δt_{DEM}, optimizes the model. This approach results in only a 2.2% error in overall collision detection while reducing DEM computational time by nearly 70%. The framework had been validated in case of a rotating drum granulator and mixer, where the dynamics of agglomeration was predicted adequately.

In the bi-component granulation processes, granular particles are typically of three types: pure API, pure excipient, and mixed granules. Consequently, to simplify and model the internal physical properties of any granule type in DEM simulation, we considered the weighted volumetric mean of API and excipient properties, accounting for their respective contributions. Note that, this approach is only considered for the coefficient of restitution property in all considered test cases in this article .

Moreover, to verify the growth formulation (9) due to addition of liquid droplet in the coupling framework, several DEM simulations are conducted incorporating liquid droplets as granular particles. The details of these simulations and the output from these simulations are provided in Section 3.1.

2.3. PBM-DEM coupling framework

From the introductory discussion, it is evident that DEM and PBM alone are insufficient for accurately and efficiently modeling granulation processes. Therefore, we present the following bi-directional multi-component PBM-DEM coupling framework. The schematic of the proposed PBM-DEM coupling algorithm is presented in Fig. 2. The PBM component is solved using MATLAB, while DEM simulations are performed with the open-source LIGGGHTS-Public software. The simulation begins with setting up the equipment geometry and meshing in Gmsh, a 3D finite element mesh generator with built-in pre- and post-processing capabilities. Next, particles are initialized and settled within the equipment geometry without agitation. Following gravitational settling, agitators start rotating and agitate the particles. Once the system reaches a steady state, collision data extraction begins. In this framework, DEM simulates non-cohesive granular particles and extracts collision frequency matrices at different time points, where each matrix entry represents the collision frequency between two particle size classes. The particle classes contain both pure solid components (API and excipient) and mixed aggregates. The extracted collision frequency matrix is then transferred to the PBM to formulate the updated aggregation kernel (β). Then, PBM is simulated to advance the process time and determine the corresponding size and composition-based distribution of particles within the granulator. During PBM simulation, particle sizes and compositions evolve due to collisional aggregation and growth resulting from liquid binder addition. The details of these models have been discussed earlier in this section. Subsequently, the updated particle size distribution (PSD) transferred back to the DEM and we initiate a new DEM simulation using this updated PSD, rather than modifying particle sizes mid-simulation. This approach avoids unphysical overlaps and abrupt changes in contact forces that could result from sudden radius inflation of particles already in contact. By reinitializing the DEM with the new particle sizes and allowing the system to evolve to a steady state – monitored through kinetic energy convergence – we ensure that particle configurations remain physically realistic. Now, further calculation of collision frequencies take place and this collision information is again transferred to PBM. This coupling framework is built upon the bi-directional frameworks proposed by Das et al. [15] and Barrasso et al. [32].

The coupling timeline of the proposed bi-directional PBM-DEM framework is illustrated in Fig. 3. Given that DEM simulations are computationally expensive, the proposed framework utilizes DEM solely for

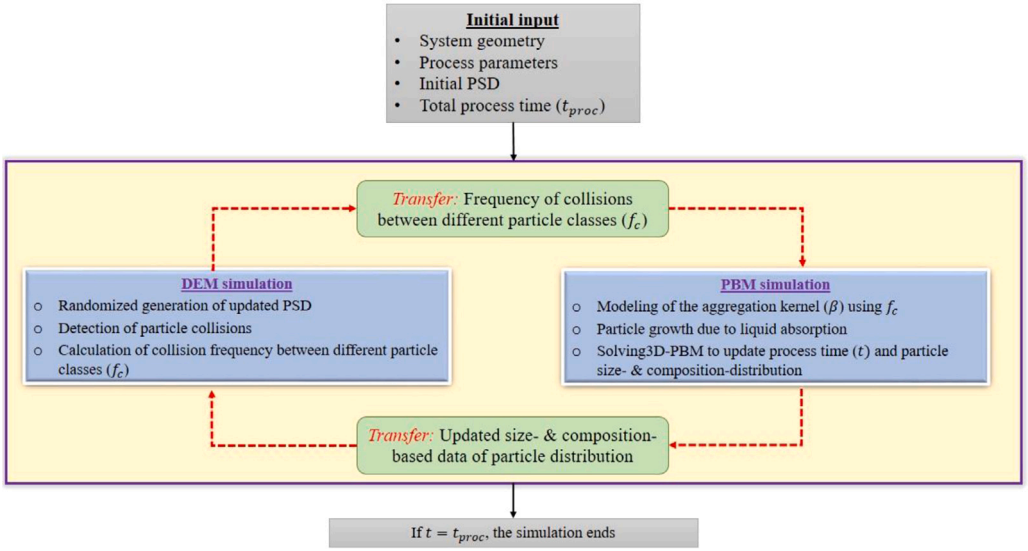

Fig. 2. Proposed bi-directional PBM-DEM coupled framework.

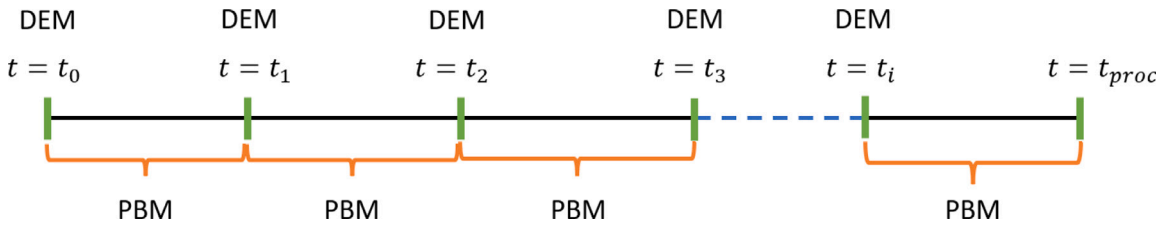

Fig. 3. Timeline overview of the bi-directional PBM-DEM coupling methodology.

stationary simulations, where the process time remains frozen. Moreover, PBM simulations are only employed for advancing the process time, thereby enhancing computational efficiency. PBM simulations persist until a predefined trigger condition for DEM is met. In our test cases, this trigger is either a 20% change in the average particle volume or the passage of a specified time period [15,32].

While this PBM-dominant PBM-DEM coupling is computationally less expensive than direct DEM simulations due to limited number of DEM runs, Das et al. [15] demonstrated that for one-dimensional systems, the DEM component still consumes almost all of the computational time. This issue can be exacerbated for larger or industrial-scale systems. Thus, there is an urgent need to develop a new adaptive DEM simulation technique that adjusts the DEM simulation box size based on requirements while preserving accuracy and efficiency. Such an approach can effectively control the overall DEM computational expense and reduce overall computational time.

2.3.1. *Adaptive system scaling method (ASSM)*

Due to the presence of large number of particles in industrial-scale systems, conducting DEM simulations on standard CPUs remains a significant challenge. Possible solutions include zooming into characteristic subdomains or simulating for shorter time intervals. Another interesting approach is to reduce the computational time by scaling down [39] the overall system without altering the size of individual particles. This approach enables simulation with reduced mass and a more manageable number of particles, thus reducing overall computational time significantly. As the size of the particles is not reduced in the scaled-down system, the original particles are treated as coarse-grained (CG) particles. For example, if the simulation system is scaled down by a factor of l in each direction, the total system volume is reduced by a factor of l^3, while particle sizes remain unchanged. Consequently, particle sizes in the scaled system are l times larger than expected, where l is defined as the system's coarse-grained ratio.

In the DEM simulations integrated within the proposed PBM-DEM coupling framework, we use a scaled-down system. This approach simulates a reduced number of particles while retaining their actual size to ensure the volume fraction remains consistent with that of the original, fully resolved system. Such scaling enables efficient computational handling without compromising the physical accuracy of the simulated particulate interactions. As particles undergo aggregation and growth during wet granulation, leading to an increase in the average particle size over time. The geometric dimensions of the DEM system must be adjusted dynamically during the operation of the coupled framework to ensure consistency in the system's solid volume fraction. We refer to this technique as the dynamic Adaptive System Scaling Method (ASSM). In such a scaled system, the collision frequency among particle size classes may decrease due to the presence of fewer particles. Consequently, to maintain the accuracy of predictions, collision frequencies between different particle size classes derived from scaled-down simulations must be appropriately scaled to reflect those of the original system. This scaled collision frequency is crucial for successfully coupling DEM and PBM, ensuring accurate information transfer between the two models.

Scaling down a system treats original-sized particles as coarse-grained, requiring adjusted collision frequencies for accurate transfer to

PBM. Proper scaling, as demonstrated by De et al. [28], ensures consistency despite differences in collision counts between CG and resolved systems. The collision frequency per unit volume of the system ($f_{c,tot}$) can be estimated from the kinetic theory of granular flows [40,41]:

$$f_{c,tot} = 4\, n^2\, d_p\, \sqrt{\pi\theta}\, g_0(\epsilon_g) \tag{15}$$

where n denotes particle number density with diameter d_p, while g_0 and θ stand for the radial distribution function and one-third of the mean square velocity, respectively. Note that both g_0 and θ remain constant during the transition from resolved to coarse-grained particles due to unaffected mass and volume of parent particles. The scaling relationship between resolved and coarse-grained systems, denoted by superscripts Res and CG respectively, is governed by:

$$d_p^{CG} = l\, d_p^{Res} \quad \text{and} \quad N^{Res} = l^3\, N^{CG}. \tag{16}$$

As a result, the ratio of collision frequencies between resolved and coarse-grained systems is given by:

$$\frac{f_{c,tot}^{Res}}{f_{c,tot}^{CG}} = \left(\frac{N^{Res}\, d_p^{Res}}{N^{CG}\, d_p^{CG}}\right)^2 = l^4. \tag{17}$$

This equation demonstrates that the total collision frequency in the resolved system is l^4 times that of the coarse-grained system, necessitating an l^4 scaling for the coarse-grained system's collision frequency to match that of the resolved system, as validated by De et al. [28]. In this article, we propose a similar approach to De et al. [28]. For instance, suppose we aim to simulate only N_{scaled} particles in DEM simulations within the coupled framework, where N_{orig} represents the total number of particles in the original (read as resolved) system at the initial time ($t = t_0$). To maintain the same fill level, the system must be scaled down by a factor of $(N_{orig}/N_{scaled})^{1/3}$ in each direction. This scaling factor, denoted as l_0, represents the coarse-grained ratio for the first iteration in the PBM-DEM coupled framework. Thus,

$$l_0 = \left(\frac{N_{orig}}{N_{scaled}}\right)^{1/3}. \tag{18}$$

The collision frequency between different particle sizes obtained from the first iteration is scaled by l_0^4 before transferring to PBM. As the PBM-DEM coupled framework progresses, the average particle radius increases during aggregation. Let r_i represent the average radius of particles in the ith iteration, with the initial average radius denoted as r_0. To maintain a constant total number of particles (N_{scaled}) in subsequent iterations, the system must be scaled by

$$l_i = \left(\frac{N_{orig}}{N_{scaled}}\right)^{1/3} \frac{r_i}{r_0}. \tag{19}$$

Once again, collision frequency must be scaled by l_i^4 before sharing it with PBM. Clearly, the system dimension in DEM during the PBM-DEM coupled framework will be adaptive to keep the total number of particles fixed and will be changed dynamically depending on the average size of particles in the system. These DEM simulations with adaptive geometries will be called adaptive DEM simulations in this article. Verification of this proposed method is provided in Section 3.

3. Verification of proposed models: Growth due to liquid absorption and adaptive system scaling method (ASSM)

This section is dedicated to the verification of proposed new models in the previous section. Firstly, we will discuss about the correlation between liquid addition rate and their absorption rate. Consequently, we will also present a concrete discussion on the proposed ASSM technique.

Table 1
Values of granular material properties, liquid droplet properties and system information used in the impeller-bowl simulation.

Particle properties and system information	Granular particles	Liquid droplets
Density of particle (kg/m^3)	1668	1000
Poisson's ratio (ν)	0.055	0.1
Coefficient of restitution (e)	0.3	0.01
Coefficient of static friction (μ_s)	0.5	0.1
Coefficient of rolling friction (μ_r)	0.1	0.01
Diameter of liquid droplets (μm)	–	190
Young's modulus (Pa)	5×10^6	
Time for settling the particles (s)	1	
DEM time step (Δt_{DEM}) (s)	10^{-6}	
Impeller rotational speed	60 rpm	

3.1. Liquid absorption rate

In this study, our goal is to efficiently incorporate liquid droplets into the PBM-DEM coupled framework. A method demonstrated by Barrasso et al. [1] involves treating droplets as granular particles within DEM, assigning them specific properties such as density and restitution coefficient. These droplets are removed upon interaction with solid particles, with their effects recorded as liquid accumulation, which is accounted for in PBM at each coupling interval. However, managing these liquid particles post-collision and tracking liquid absorption data pose significant computational challenges.

To address these challenges, we establish a correlation to model liquid addition and absorption by different size classes using some DEM simulations. This correlation can be directly integrated into PBM, eliminating the need to simulate liquid addition in DEM during the coupling process of DEM and PBM. The Hertz–Mindlin contact model is used for droplet–droplet interactions. To establish the relationship between absorbed liquid quantity and various size classes, we conducted numerous DEM simulations with various PSDs. In these simulations, droplets, with a density equivalent to water, were modeled as solid particles. Unlike in reality where the droplets merge, these simulated liquid droplets deflect upon collision with each other, behaving like granular particles. We assigned a very low coefficient of restitution (0.01) to the droplets to ensure they mimic the agglomeration of liquids by staying close after collisions. When a droplet collides with a granular particle, it is removed from the system, and the particle's liquid content increases, representing absorption without applying contact forces. In these simulations, particles were initially placed within a bowl and impeller system, allowed to settle for a duration of 2 s. Subsequently, rotation of the impeller commenced, initiating the generation of a stream of liquid droplets from a predetermined height above the particle bed. Within our investigation, the liquid droplets were represented as granular particles within the DEM framework. The properties associated with these liquid droplets are detailed in Table 1.

A total of 85,000 water droplets were introduced for each simulation involving various PSDs. To execute this simulation, the source code of LIGGGHTS-Public [42] has been modified. Our code is implemented in the compute_contact_atom.cpp file inside the source folder 'src' of LIGGGHTS-Public.

Various PSDs have been examined in the conducted DEM simulations. The characteristics of granular particles and the dimensions of the impeller-bowl system are detailed in Table 1 and Fig. 4, respectively. We have explored multiple scenarios regarding the absorption of liquid by the particles. In the first case, granular particles fully absorb liquid droplets upon contact. In the second case, certain size classes exhibit conditional absorption upon encountering liquid droplets. These scenarios will be explained further in the subsequent cases. A schematic representation of this liquid absorption approach is depicted in Fig. 5.

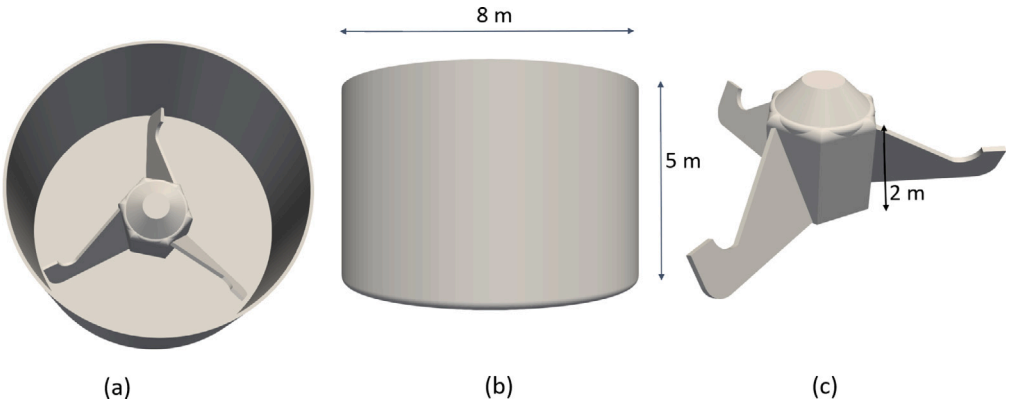

Fig. 4. System Dimensions of the granulator.

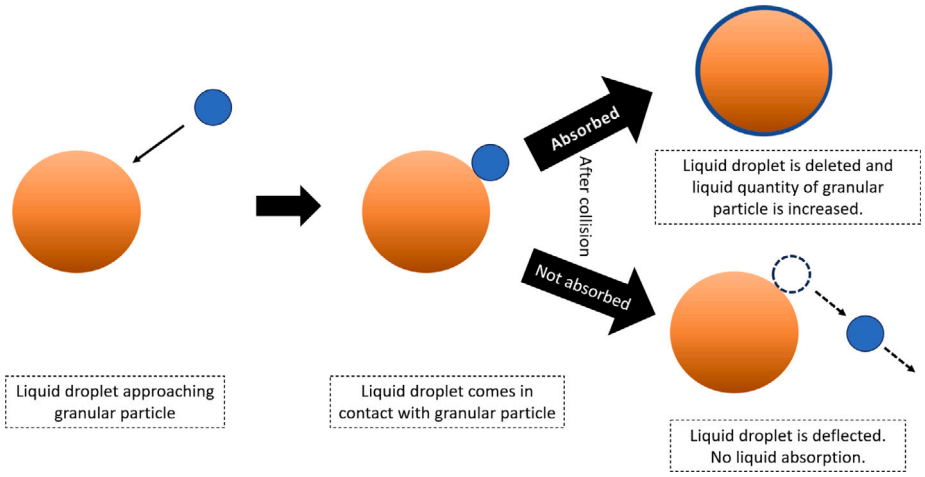

Fig. 5. Graphical representation of complete (test case 1) and conditional (test case 2) absorption of liquid droplet in DEM simulation. In the complete absorption case (test case 1), all the liquid droplets are absorbed by the granular particles successfully upon the contact, which is not the case for test case 2.

3.1.1. *Test case 1: Complete absorption of liquid*

In this particular case study, we assume that granular particles completely absorb all the liquid droplets upon contact, as depicted in Fig. 5. Five distinct PSDs are considered, as shown in Fig. 6. These PSDs, namely D1, D2, D3, D4, and D5, span sizes ranging from 100 μm to 625 μm, each adhering to a Gaussian distribution with unique mean (260, 320, 380, 440, and 500 μm, respectively) values and same standard deviation of 100 μm. As the impeller rotates and liquid droplets are introduced, granular particles undergo agitation, while the droplets descend onto the granular bed. Upon contact with granular particles, the liquid droplets are absorbed, consequently augmenting the liquid content within the particles. The snapshots of the initial stage (following settling of granular particles) and the final stage (post-absorption of liquid droplets) are illustrated in Figs. 7 and 8. Additionally, the coloration of granular particles in Fig. 7 indicates the extent to which individual granules have absorbed liquid droplets. Figs. 8(a) and 8(b) show the different radii of particle in different colors at the start and end of the simulation.

The rotation of the impeller induces agitation among the granular particles within the bowl, facilitating concurrent particle mixing. Animation (Animation1.avi) in the supplementary material illustrates the DEM simulation of liquid droplet absorption. Sub Fig. 9(a) illustrates the total liquid absorption across various particle size classes. Sub Fig. 10(a) plots the liquid absorption per unit volume of granules across various size classes, while sub Fig. 9(a) displays only the number normalized liquid absorption for each particle class. The findings depicted in Fig. 10(a) reveal a linear correlation between the volume of particle

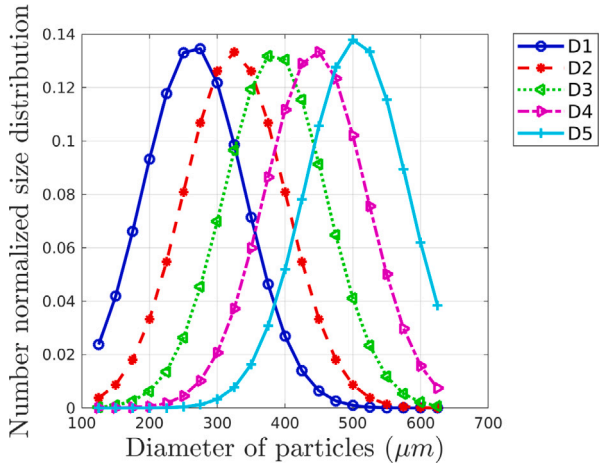

Fig. 6. Different PSDs used in the test case simulations to verify liquid absorption rate.

size classes and the accumulated liquid. Consequently, a cubic curve has accurately predicted the observations of different considered PSDs. This observation underscores a discernible relationship between the volume of granular particles of different size classes and the quantity of absorbed liquid droplets. To strengthen our claim, we have also performed some simulations for the same PSD where the particle static friction (μ_s) and coefficient of restitution (e) have been changed to

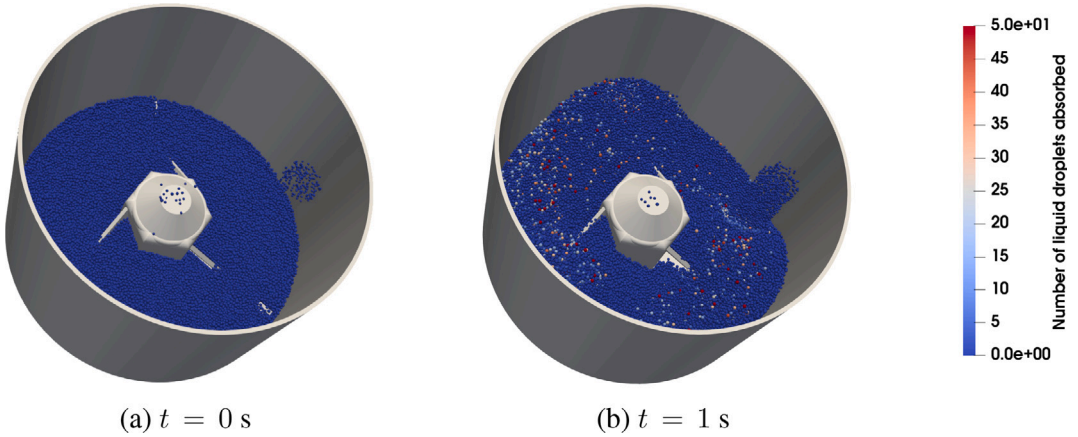

Fig. 7. Comparison of initial (a) and final (b) snapshots of the DEM simulation for PSD D5 for test case 1. The colors represent the amount of liquid absorbed by different particles based on the color bar provided on the right.

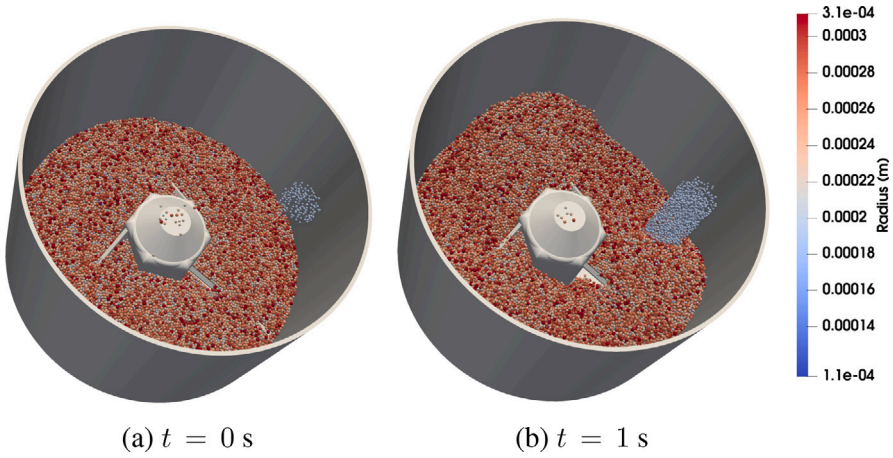

Fig. 8. Comparison of initial (a) and final (b) snapshots of the DEM simulation for PSD D5 for test case 1. The colors represent the radii of different particles as provided on the color bar on the right.

0.3 and 0.1, respectively. The results obtained from these simulations have been displayed in Figs. 9(b) and 10(b). The results show a good agreement between the proposed model and the simulation results.

3.1.2. Test case 2: Conditional absorption of liquid droplets

In real-world situations, certain granular particles exhibit hydrophobic behavior, causing them to repel liquid droplets upon contact. The second test case investigates this phenomenon, focusing on how specific particle size classes, due to their hydrophobic properties can affect the absorption of liquid droplets. In these simulations, we have considered similar granular particle size classes as test case 1. Also, we assumed that alternative size classes (i.e., size classes with diameters 125, 175, 225, ⋯, 625 μm) have a ψ% probability to absorb liquid droplets while remaining size classes will absorb 100% liquid droplets during collisions. If a granular particle fails to absorb the liquid droplet after a collision, the droplet is redirected with post-collisional velocity. Fig. 5 illustrates this process visually.

For instance, when a liquid droplet comes into contact with a granular particle, there is an ψ% chance of absorption by the granular particle. Subsequently, based on predefined conditions, the droplet is either absorbed entirely or deflected for another collision with a different granular particle in the system. This deflected droplet can merge with other particles. To simulate this behavior, we modified the source code of the DEM simulation software, LIGGGHTS-Public. During each collision between a liquid droplet and the specified granular particle size classes, a uniformly distributed random number between 0 and 1 is generated. If this random number is less than $\psi/100$, the collision is deemed successful, and the liquid droplet is absorbed by the granular particle. Otherwise, the droplet is deflected for another collision.

For this particular test case, we ran a DEM simulation where granular particles with specific size classes absorbed $\psi = 50\%$ of liquid droplets upon contact. Three different PSDs, D3, D4 and D5 (Fig. 6), are taken into consideration in this test case 2. Consequently, after DEM simulations, the calculated amount of liquid absorbed is normalized with each particle class, number, volume, and absorption probability to determine the correlation with particle size. The outcomes are illustrated in Figs. 9(c) and 10(c). Similar to the previous test case, the results were well matched against a cubic curve with the proportionality constant mentioned in (7). An additional test case was performed in which the liquid absorption probability, ψ, was set to 70% for alternating particle size classes. Simulations were carried out for the D1, D2, D3, D4, and D5 PSDs. The corresponding results are presented in Figs. 9(d) and 10(d). A strong agreement is observed between the simulation outcomes and the predictions of the proposed model.

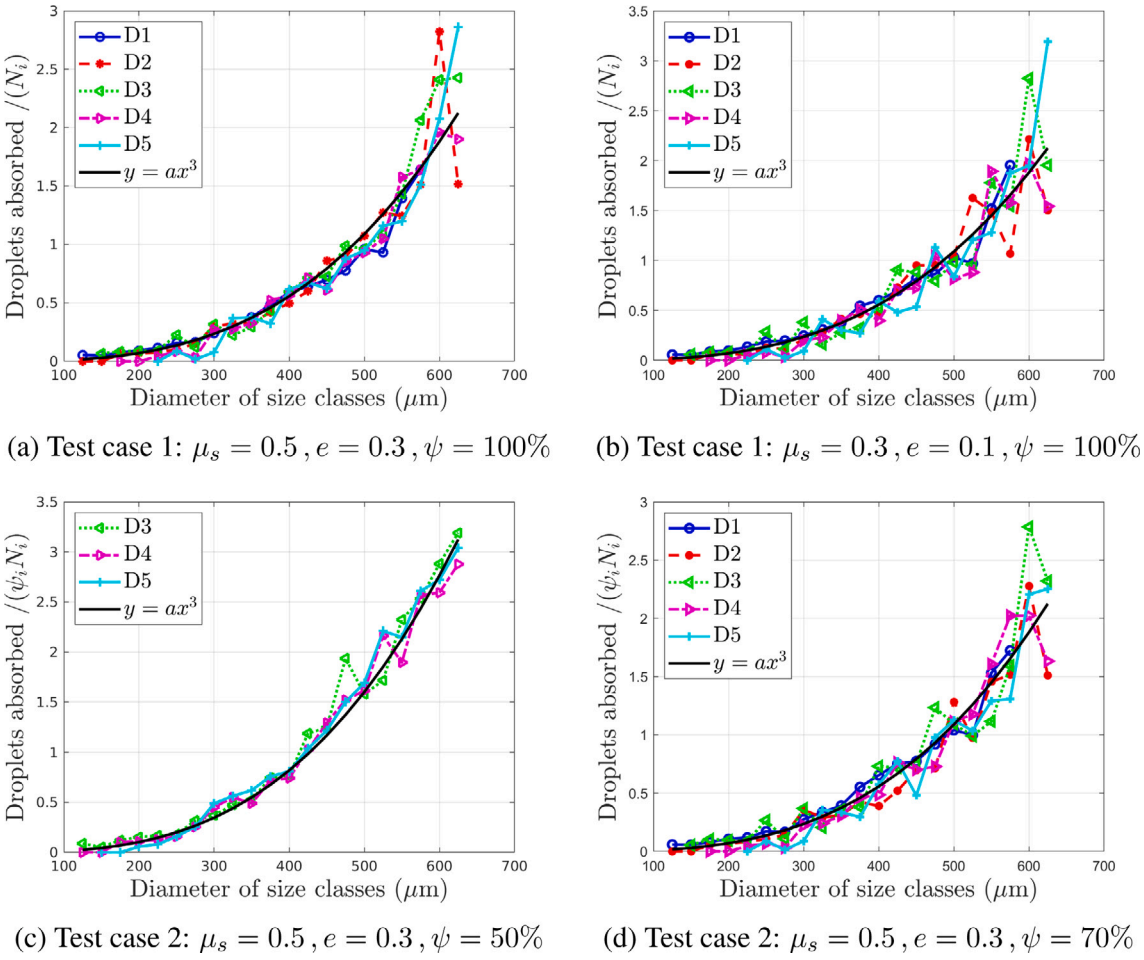

(a) Test case 1: $\mu_s = 0.5\,, e = 0.3\,, \psi = 100\%$

(b) Test case 1: $\mu_s = 0.3\,, e = 0.1\,, \psi = 100\%$

(c) Test case 2: $\mu_s = 0.5\,, e = 0.3\,, \psi = 50\%$

(d) Test case 2: $\mu_s = 0.5\,, e = 0.3\,, \psi = 70\%$

Fig. 9. Distribution of number normalized absorbed liquid on different particle classes when (a) the liquid droplets are completely absorbed with $\mu_s = 0.5\,, e = 0.3$, (b) the liquid droplets are completely absorbed with $\mu_s = 0.3\,, e = 0.1$, (c) the chance of absorption of liquid droplets is 50% for alternative size classes, and (d) the chance of absorption of liquid droplets is 70% for alternative size classes.

This discussion highlights that the absorption of liquid droplets depends on the volume of particle size classes in the simulation. A proposed law based on Eq. (7) accurately predicts the number of droplets absorbed by each size class. This law can be directly incorporated into PBM, offering computational efficiency. To demonstrate this efficiency, we conducted simulations with (complete absorption of liquid) and without liquid droplets. Specifically, in a simulation with PSD D3 with 100,000 particles, we solely performed particle settling and rotation without introducing liquid droplets. The comparison of simulation duration is shown in Table 2, revealing a significant reduction (more than 24%) when liquid droplets are excluded in DEM. This efficiency gain is attributed to the reduction of computational resources consumed by continuous droplet addition and deletion processes, which involve neighbor calculations and periodic recreation of neighbor lists. Another aspect of the high computational cost consumption is the presence of a large number of particles in the simulation for industrial-scale systems. To address this challenge, we have proposed an adaptive system scaling method in Section 2.3.1, whose accuracy and efficiency is discussed in the following subsection.

Table 2
Comparison of computational time for with and without introducing the liquid droplets in the DEM simulation.

	Computational time (h)
With liquid droplets	6.5
Without liquid droplets	4.8

3.2. Verification of adaptive system scaling method (ASSM)

As detailed in Section 2.3.1, effective system scaling is crucial for reducing computational time without sacrificing accuracy. The concept involves conducting DEM simulations with fewer particles at their original sizes, ensuring computational feasibility. In our PBM-DEM coupled framework, we advocate the use of a fixed number of particles in DEM simulations for any given PSD. This reduced particle count should be substantially lower than the original system's count. To achieve this, we propose to scale down the system by a factor of $l_i = \left(N_{orig}/N_{scaled}\right)^{1/3} \cdot r_i/r_0$, where l_i, i, N_{orig}, N_{scaled}, r_i, and r_0 represent the coarse-grained ratio of the system, the PBM-DEM coupling iteration number, the actual number of particles in the original system, the fixed number of particles used in the DEM simulation in the coupled framework, the average radius at the ith iteration, and the initial average radius of the system, respectively. As we scale down the system's geometry while keeping particle sizes constant, the particles within the simulation domain must be treated as coarse-grained particles. Collision frequencies between different size classes obtained from coarse-grained DEM simulation need to be rescaled by l_i^4 before transferring to PBM to adjust for smaller number of collisions resulting from coarse-grained particles [28].

To verify the accuracy and efficiency of this proposed dynamic system scaling technique, we applied this proposed method to mixer-impeller systems within a univariate PBM-DEM coupling framework

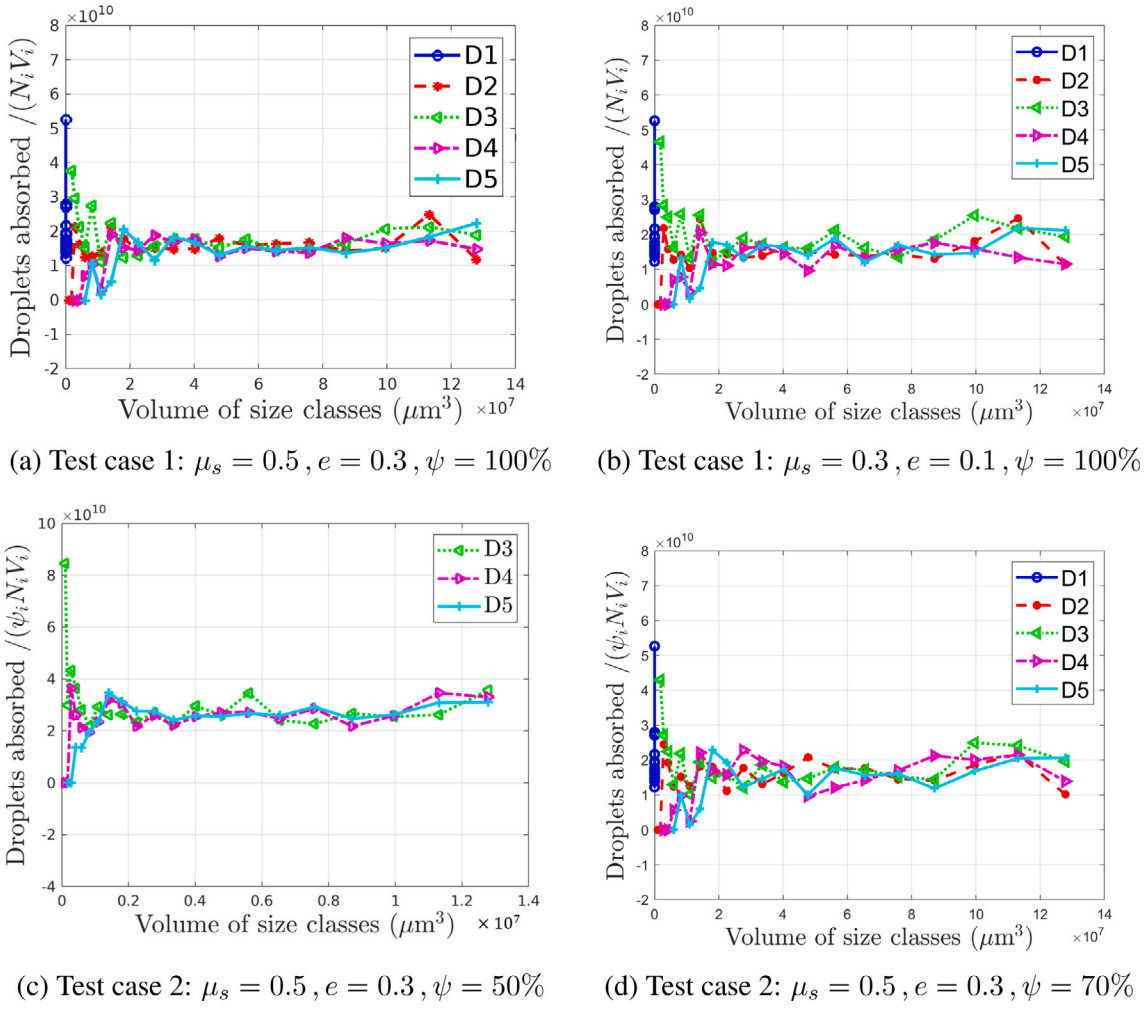

(a) Test case 1: $\mu_s = 0.5\,, e = 0.3\,, \psi = 100\%$

(b) Test case 1: $\mu_s = 0.3\,, e = 0.1\,, \psi = 100\%$

(c) Test case 2: $\mu_s = 0.5\,, e = 0.3\,, \psi = 50\%$

(d) Test case 2: $\mu_s = 0.5\,, e = 0.3\,, \psi = 70\%$

Fig. 10. Distribution of absorbed liquid droplets (per unit volume) on different particle classes (a) the liquid droplets are completely absorbed with $\mu_s = 0.5\,, e = 0.3$, (b) the liquid droplets are completely absorbed with $\mu_s = 0.3\,, e = 0.1$, (c) the chance of absorption of liquid droplets is 50% for alternative size classes, and (d) the chance of absorption of liquid droplets is 70% for alternative size classes.

[15]. The system dimension is illustrated in Fig. 4. Initially, the system was partially filled with mono-sized volume 10 mm^3 with a density of 1,000 kg/m^3, which constitutes a total granular mass of 1.5 kg. Moreover, we consider that during aggregation, these particles grow up to the volume of 200 mm^3. No liquid droplets were introduced in this simulation for simplicity, and other particle properties remained consistent with those listed in Table 1. With this setup, the univariate PBM-DEM framework is simulated up to 300 s of process time for the three following cases:

- Resolved simulation with 150,000 particles, serving as a reference simulation.
- Coupling simulation with ASSM technique with appropriate scaling of collision frequencies. For each of the DEM iterations, the number of particles inside DEM is fixed to 15,000.
- Coupling simulation with ASSM without scaling the collision frequencies.

Fig. 11, 12, and 13 presents a comparison of results from three simulations. In the left column of Figs. 11 and 13, we compare resolved coupled simulation with ASSM enabled coupled simulation without scaling collision frequency. Figs. 11 and 13 depict the mass and number of particles for different size classes at various timestamps, alongside the mean volume and total number of particles shown in Figs. 12(a) and 12(b). In contrast, Figs. 11(b), 12, and 13(b) compare resolved coupled simulation with ASSM, incorporating proper scaling of collision frequency. The comparison reveals the significance of scaling collision frequency when implementing ASSM. Properly scaled collision frequency leads to highly accurate predictions of mass and number of particles across various size classes compared to the ASSM case without scaled collision frequency. Therefore, these results underscore the importance of scaling collision frequency for obtaining accurate predictions of real systems. Table 3 shows the errors in computing mass of particles at different timestamps with and without scaling f_c. Cleary, ASSM without scaling f_c produces enormous error whereas the ASSM with proper scaling produced results with error less than 6%.

If only pure PBM simulation is executed, it will take a computational time of around 127 s to complete the simulation of 200 s. However, it does not take into account the effects of intermediate change in collision frequency between different size classes from DEM in PBM-only simulation. Thus, the comparison of computational time between “PBM-only” simulation and PBM-DEM coupled simulation is not appropriate. Therefore, the comparison of computational times for resolved and ASSM are presented in Table 4. One can observe that the computational time for ASSM is reduced by almost 83% compared to the resolved simulation.

The reduced number of particles remained to be 15,000 for DEM to verify ASSM method, but, a change in the number of particles will change the computational expenses. The number of particles is to be such that it has to be statistically sufficient as well as optimized in

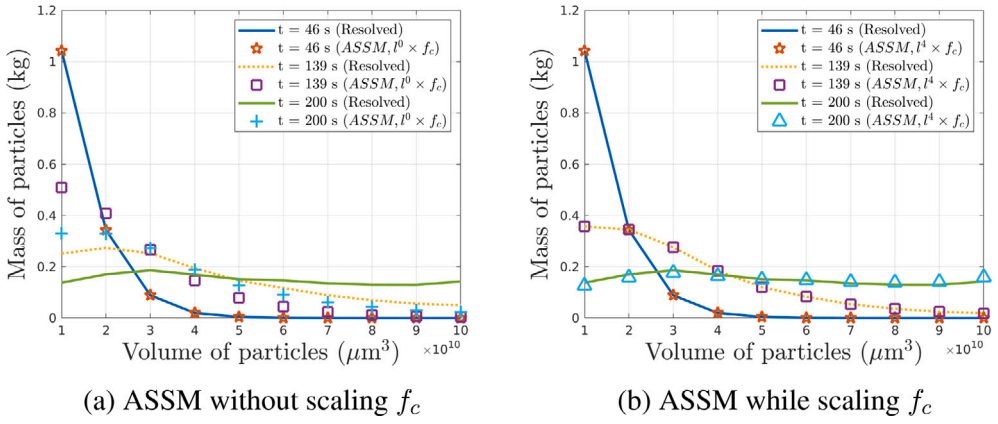

Fig. 11. The effect of proper scaling of collision frequency in PSD.

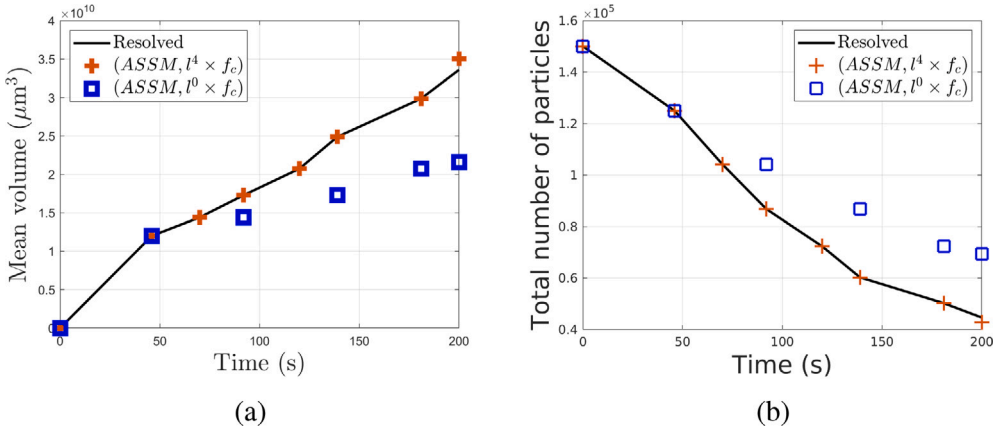

Fig. 12. The effect of proper scaling of collision frequency in the evolution of (a) mean volume and (b) total number of particles.

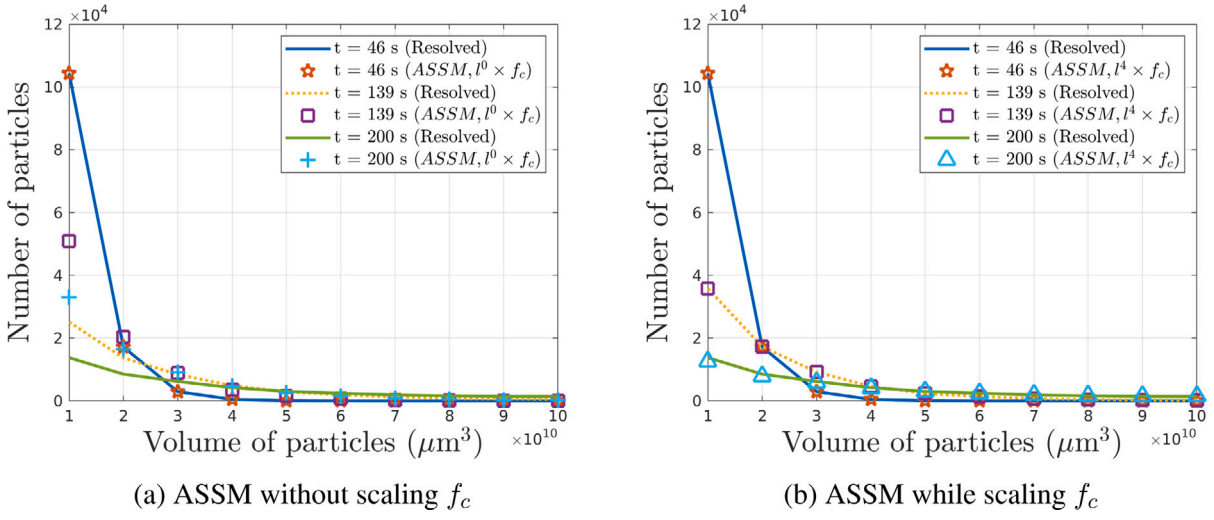

Fig. 13. The effect of proper scaling of collision frequency in PSD.

Table 3
Comparison of errors in ASSM with and without scaling f_c.

Simulation type	Error (%) at t = 46 s	Error (%) at t = 139 s	Error (%) at t = 200 s
ASSM, $l^4 \times f_c$	0	0.0001	5.7533
ASSM, $l^0 \times f_c$	0	58.75681	62.60090

Table 4
Comparison of computational time between Resolved (full scale) and ASSM DEM simulation.

Process time (s)	Resolved simulation (Comp. time (Hours))	ASSM simulation (Comp. time (Hours))
100	2.121	0.383
200	4.677	0.810
300	6.410	1.117
400	8.226	1.438
500	10.962	1.912

Table 5
Comparison of computational time between different ASSM simulations for different numbers of particles.

Number of particle for ASSM	Computational time (h)	Error (%) in mean volume after 200 s
5,000	1.421	15.252
15,000*	1.912	2.781
25,000	2.569	0.976
50,000	4.149	0.611
100,000	5.625	0.426
150,000	10.962	0.0

terms of computational cost. To justify our claim, the ASSM simulations were simulated for 5,000, 25,000, 50,000, and 100,000 particles and compared the computational time in Table 5. It is evident that increasing the number of particles leads to higher computational expense. Thus, ASSM simulation with 15,000 number of particles is taken into consideration.

4. Results and discussion: Adaptive PBM-DEM coupling framework

In the preceding section, the efficiency and accuracy of the proposed PBM-DEM coupling framework were demonstrated. This section details the validation of the framework and its applicability to various wet granulation setups. Initially, the model is validated against the experimental granulation results reported by Poon et al. [43]. Subsequently, we explore the effects of variation in the liquid-to-solid ratio and binder addition rate on the bowl-impeller granulation system.

4.1. Validation of proposed PBM-DEM coupling framework

To validate our proposed methodology, we referenced the experimental results reported by Poon et al. [43]. The system dimensions and particle parameters align with those described in the studies of Poon et al. [43] and Ramachandran et al. [44]. The initial mean diameter of the particles was set at 130 μm, with binder liquid sprayed at a rate of 1.72 mL/s. To replicate the experimental setup of single solid component, we restricted our proposed model (1) to $s_2 = 0$. The values of adjustable parameters in the Madec kernel (4) were calibrated to $\alpha = 1$, $\delta = 1$ and $\beta_0 = 2\times10^3$. In our simulation, we used a fixed number of 50,000 particles in ASSM DEM simulations. DEM simulations were triggered at intervals of every 5 min within this coupled framework for a total process time of 15 min.

While the proposed framework is capable of replicating the outcomes for all test cases presented by Poon et al. [43], this paper focuses on a comparative analysis with test case 1 only. The evolution of the mean particle diameter and the final Particle Size Distribution (PSD) at $t = 15$ min are illustrated and compared against the experimental data in Figs. 14(a) and 14(b), respectively. The simulated results have shown meticulous agreement with the experimental data. Importantly, our model successfully captures the overall bi-modal nature of the PSD, reflecting its ability to reproduce essential granulation characteristics. This qualitative agreement demonstrates the robustness of our framework, even though occasional discrepancies at specific size classes may arise from experimental variability or model simplifications.

Table 6
Values of properties of API, excipients and system information used in mixer simulation.

Particle properties and system information	API	Excipient
Density of particle (kg/m^3)	1668	
Poisson's ratio	0.3	
Coefficient of static friction	0.5	
Coefficient of rolling friction	0.1	
Young's modulus (Pa)	5×10^6	
Coefficient of restitution	0.9	0.1
Time for settling the particles (s)	2 s	
DEM time step (Δt_{DEM}) (s)	5×10^{-7}	
Impeller rotational speed (rpm)	240	

4.2. Application in bowl and impeller system

The developed framework can be applied to simulate a wet granulation process to predict key granule attributes such as PSD, content uniformity, and liquid content across particle classes. To assess the effects of variation in process parameters, two test examples were simulated by varying the liquid-to-solid (LS) ratio and liquid addition duration while maintaining other parameters fixed. The ensuing subsections detail the observations from these simulations. The granulator is initially loaded with 55,000 granular particles, comprising 20% pure API and 80% excipients. In our analysis, API and excipient particles are differentiated solely based on the coefficient of restitution, set to 0.9 and 0.1 respectively, to ensure sufficient variation in collision patterns. All other particle properties [45,46] were assumed to be similar and constant for simplification (see Table 6). We defined size classes each for API and excipient, resulting in a combinatorial set of mixed classes with varying API-to-excipient volume ratios. Thus, for particles containing both API and excipient, the coefficient of restitution is assigned as the weighted mean of the coefficients for API and excipient based on their respective volume fraction contributions. Thus, all other parameters of API and excipient have been kept the same, as incorporating variation in more particle properties would greatly add to the computational burden and intricacy of the DEM simulations. Both particles were initialized to a particle diameter of 58 μ m with equal mass distribution. Furthermore, it was considered that the size of each binder droplet is the same across all simulations. The parametric values of the aggregation kernel (4) are chosen to be $\alpha = 1, \delta = 1$, and $\beta_0 = 100$, respectively. During the coupling framework, DEM simulations were triggered after every 100 s of process time to update collision efficiencies and their impact on the aggregation kernel.

4.2.1. Test example 1: Variation in LS ratio

In this test example, we explore three different values of the liquid-to-solid (LS) ratio: 5%, 15%, 25%. The liquid addition duration is fixed

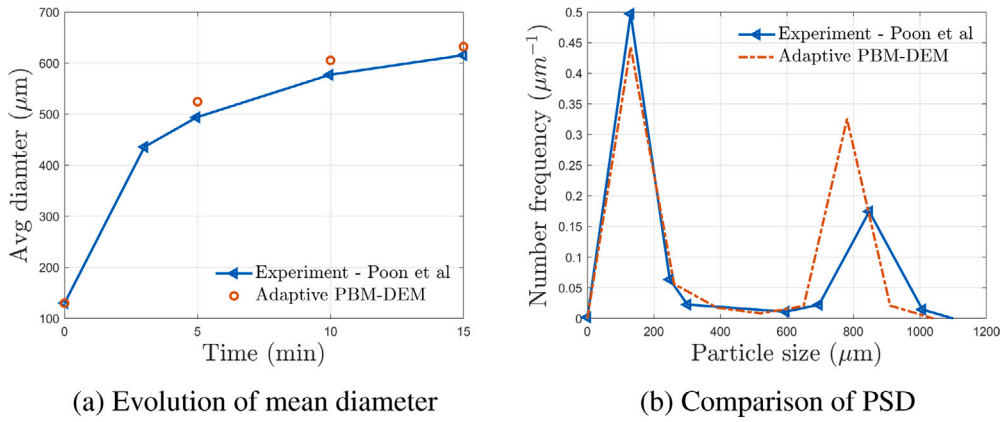

Fig. 14. Comparison of simulated and experimental (Poon et al. [43]) results at various time stamps. The drum load was 1.5 kg (case 1).

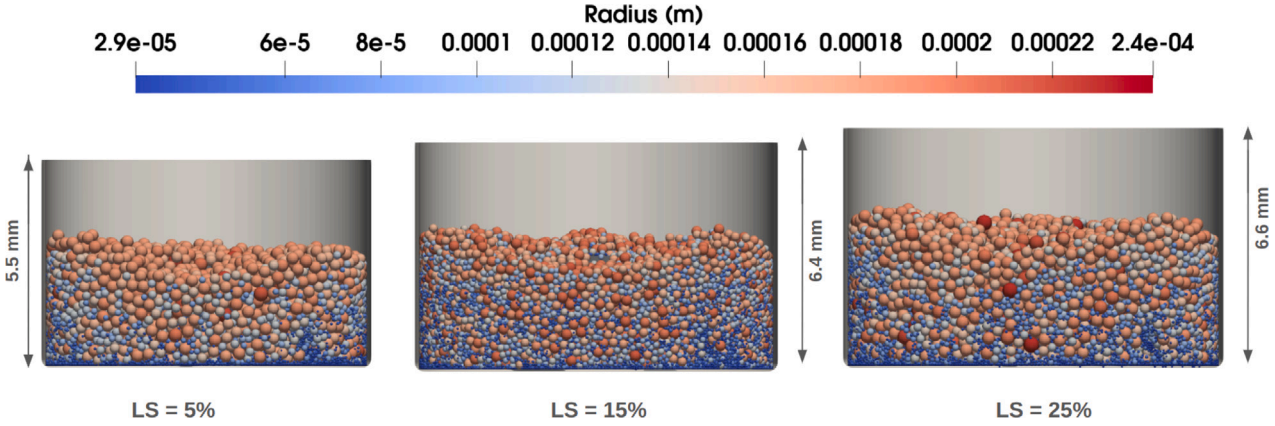

Fig. 15. Effect of system scaling during the execution of PBM-DEM coupled framework after t= 500 s.

at 50% of the total process time (t_{proc} = 500 s). The results obtained from these simulations are illustrated in Figs. 15 and 16.

During granulation, the size of the granules increases over time due to growth and aggregation mechanisms. Consequently, the adaptive system scaling method (ASSM) is employed, adjusting the size of the DEM simulation box in each iteration while maintaining a constant overall particle packing fraction. Throughout these DEM simulations, the ASSM is utilized to ensure a total of 55,000 particles within the DEM system. The evolution of the DEM system dimension for a fixed LS ratio of 15% is illustrated in Fig. 16. The system dimensions expand in line with the overall increase in particle size.

Similarly, the final system dimensions for various LS ratios are shown in Fig. 15. Similar to the previous argument, system dimension increases with the increase in LS ratio, as a higher LS ratio helps in an increased rate of aggregation and size.

The temporal evolution of various properties is depicted in Figs. 17 and 20. The evolution of average granule radius and the total number of granules in the system for different LS ratios are presented in Figs. 17(a). As expected, particles tend to aggregate and grow more in the presence of a higher amount of binder liquid. Thus, increasing the liquid content (i.e., LS ratio) should lead to an increase in the average granule size and a decrease in the total particle number. This trend is clearly observed in Figs. 17(b). Moreover, it is notable that after the liquid addition period (at 250 s), the rate of change in granule diameter and total number decreases with time due to the presence of fewer binder droplets. The time evolution of the total particle volume and the API to excipient mass ratio are presented in Figs. 20 and 17(c). While the total mass of solid components (API and excipient) remains constant over time, the total mass (or volume) of the particle system increases due to the addition of binder on the surfaces of granules. This observation is accurately illustrated in Fig. 17(c), where the increase in total volume occurs only up to the liquid addition duration, remaining constant thereafter. Furthermore, the developed framework accurately portrays the mass ratio of API and excipient components in Fig. 20, which remains constant throughout the process due to no flux in solid components.

Fig. 18 provides insights into the influence of LS ratio on the distribution of particles across various size classes. Sub Figs. 18a and 18d illustrate the number of particles within each size class relative to their respective fractional liquid content and fractional API composition for an LS ratio of 5%. The fractional liquid content refers to the ratio of liquid volume to the total volume of the particle class, while fractional API composition represents the ratio of API volume to the total volume of the particle class. Similarly, Sub Figs. 18b and 18e depict the particle distribution for an LS ratio of 15%, while Sub Figs. 18c and 18f represent an LS ratio of 25%. Notably, an increase in LS ratio results in a higher number of larger particles. Concurrently, the number of particles with greater liquid content and volume also increases with higher LS ratios, aligning with experimental trends reported in the literature [47,48].

4.2.2. Test example 2: Variation in binder addition duration

The second test case involves the study of the impact of liquid addition time on the simulation outcomes. We maintain a fixed LS ratio of 0.15 across three simulations, varying the duration of liquid addition. For each scenario, we consider liquid addition periods corresponding to 10%, 50% and 80% of the total process time. In all test cases, the total process time is t_{proc} = 500 s.

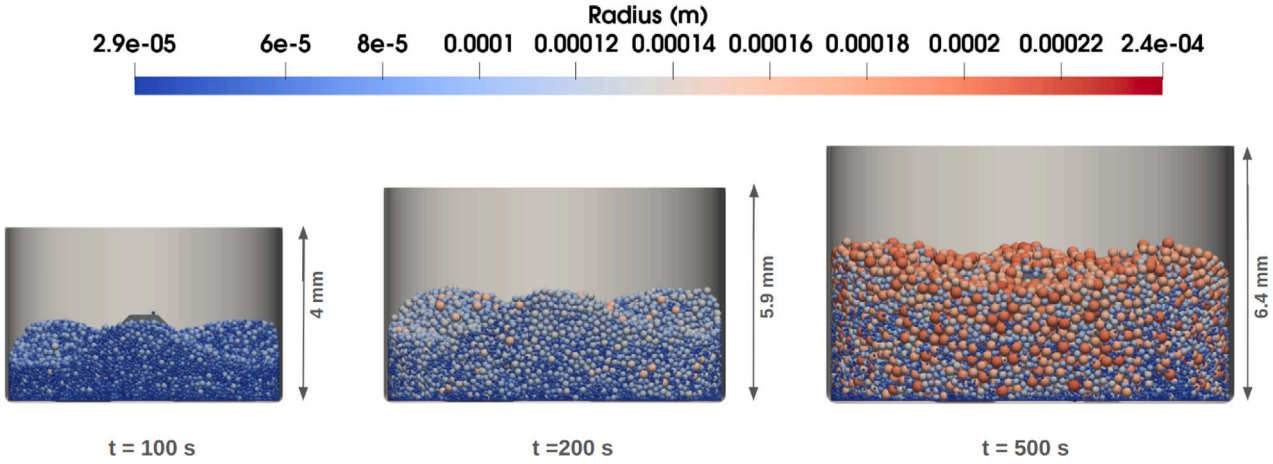

Fig. 16. The evolution of the DEM system dimension for a fixed LS ratio of 15%.

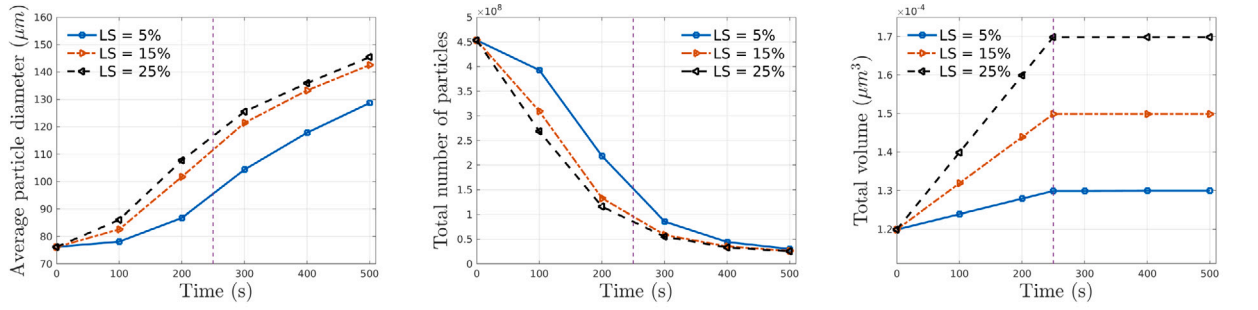

(a) Comparison of average diameter (μm) (b) Comparison of total number of particles (c) Comparison of total volume (solid + liquid)

Fig. 17. The effect of different LS ratios in the adaptive PBM-DEM coupled framework.

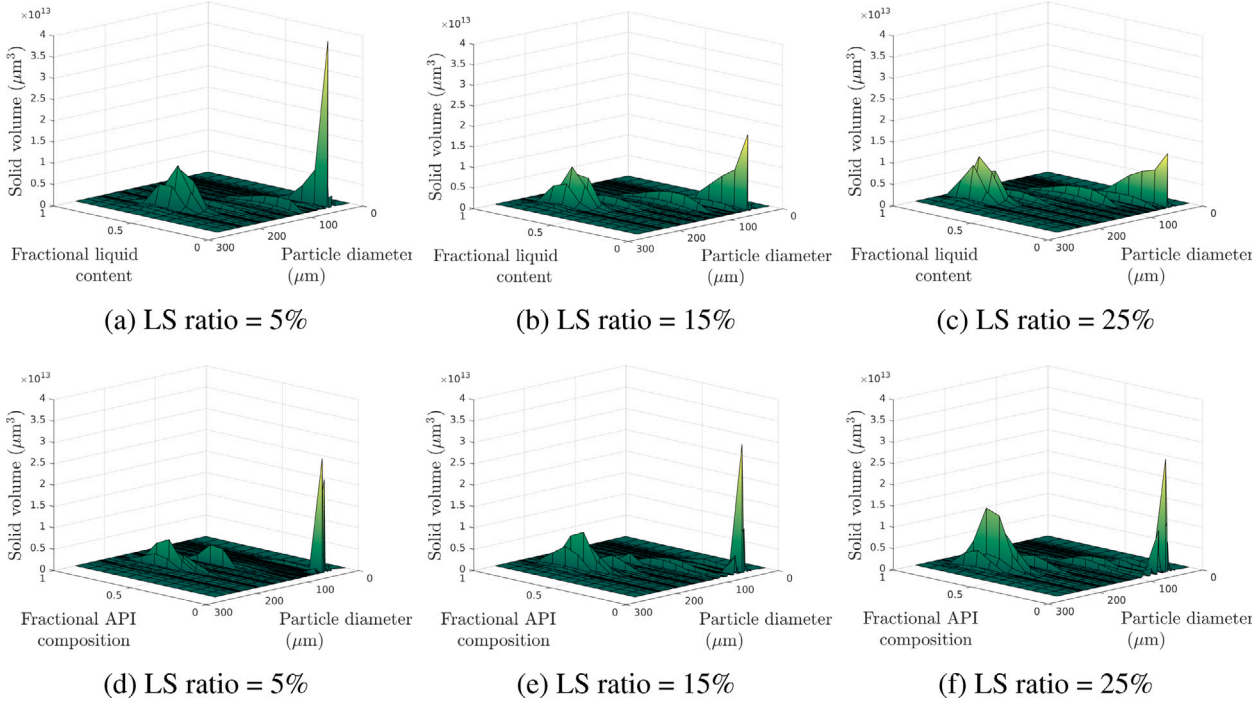

Fig. 18. The effect of LS ratio in the number of particles in the PBM-DEM coupled framework.

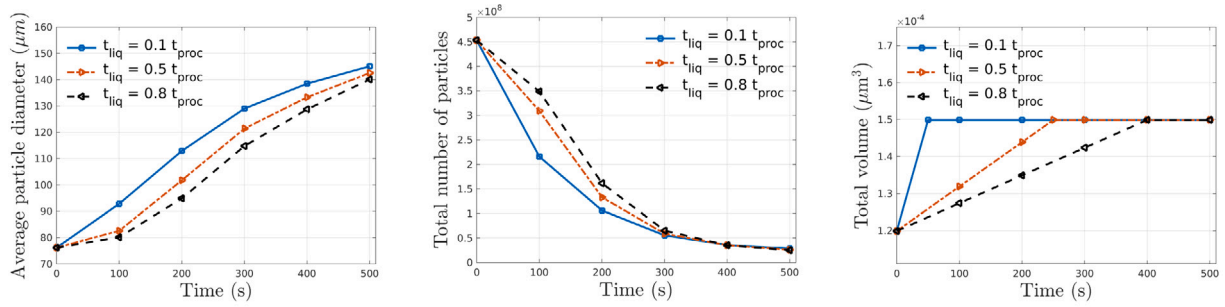

(a) Comparison of average diameter (μm) (b) Comparison of total number of particles (c) Comparison of total volume (solid + liquid)

Fig. 19. The effect of different liquid addition duration in the PBM-DEM coupled framework.

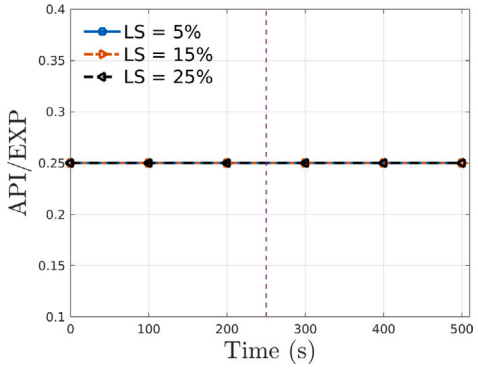

Fig. 20. The effect of different LS ratios in the adaptive PBM-DEM coupled framework: Comparison of API to excipient (EXP) mass ratio.

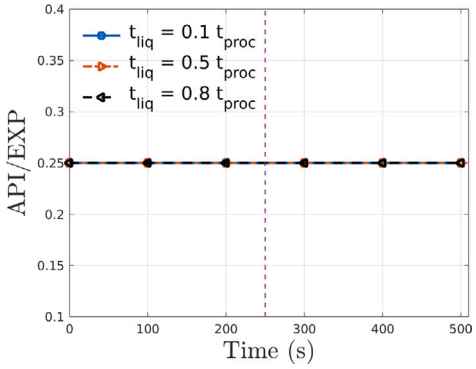

Fig. 21. The effect of different liquid addition duration in the PBM-DEM coupled framework: Comparison of API to excipient (EXP) mass ratio.

In the $t_{\text{liq}} = 0.1t_{\text{proc}}$ case, liquid addition occurs rapidly within the initial 50 s of process time. Conversely, in the $t_{\text{liq}} = 0.8t_{\text{proc}}$ case, liquid addition is gradual, spanning the initial 400 s of process time. Thus, in $t_{liq} = 0.1t_{proc}$ case, particles get liquid droplets at a rapid rate during the initial stage of the simulation, which leads to a significant rise in the average radius of the particles. On the other hand, $t_{liq} = 0.8t_{proc}$, the liquid addition occurs gradually and slowly during the simulation. Hence the average radius of the particle increases slowly in comparison to $t_{liq} = 0.1t_{proc}$ case, as shown in Fig. 19.

The temporal evolution of average particle diameter and total number of particles are plotted in Fig. 19. For the case of $t_{liq} = 0.1t_{proc}$, all of the binder liquid is inserted at the initial 50 s. Therefore, it is evident to observe a rapid rise in aggregation and growth mechanisms, resulting in a significant rise in average particle size and a decline in total particle count. This phenomenon is correctly captured in the figures. Moreover, it is also observed that for all three cases, the average particle size and total particle count tend to stabilize towards some constant value. It is because although the binder addition rate is different, the total amount of binder added is constant for all cases. Therefore, we can expect to have similar overall results for prolonged simulation of each case. Furthermore, the time evolution of total particle volumes is presented in Fig. 19(b), demonstrating that each scenario reaches a steady state but at varying process durations. Finally, in these cases, it can also be observed that the total mass ratio of the API and excipient components (see Fig. 21) remains constant throughout, validating the accuracy and consistency of the proposed simulation framework.

Finally, Fig. 22 illustrates the impact of liquid addition duration on the distribution of particles with respect to size and composition. Sub Figs. 22a and 22d represent the number of particles within each size class relative to their respective fractional liquid content and fractional API composition for liquid addition time $t_{liq} = 0.1t_{proc}$ after $t_{proc} = 500$ s. Similarly, Sub Figs. 22b and 22e present the particle distribution for $t_{liq} = 0.5t_{proc}$, and Sub Figs. 22c and 22f for $t_{liq} = 0.8t_{proc}$ after $t_{proc} = 500$ s. In all cases, all liquid droplets are fully inserted by $t_{proc} = 400$ s, resulting in qualitatively similar particle distributions by $t_{proc} = 500$ s. However, in the case of $t_{liq} = 0.1t_{proc}$, all liquid droplets are inserted within $t_{proc} = 50$ s, allowing particles more time to aggregate and form larger sizes compared to other cases. Consequently, we observe peaks (see Fig. 22a and 22b) with greater heights for $t_{liq} = 0.1t_{proc}$ compared to $t_{liq} = 0.5t_{proc}$ and $t_{liq} = 0.8t_{proc}$. Conversely, for $t_{liq} = 0.8t_{proc}$, liquid droplets are introduced more gradually, resulting in fewer particles with larger diameters generated (see Fig. 22e and 22f) during the coupled framework. This trend aligns with experimental expectations.

The above discussion highlights the effectiveness of the proposed bi-directional bi-component PBM-DEM (adaptive) coupling framework in simulating wet granulation processes. The framework demonstrates accurate and efficient predictions that align well with experimental expectations.

The validation approach utilized in this work relies on experimental data sourced Poon et al. [43], which may introduce discrepancies arising from differences in experimental conditions. Future work could address experimental validation with modified situations that better approximated the original simulated situations, they may better validate the applications of the developed mode. While the existing PBM-DEM coupling framework captures the main features of granulation dynamics, some realistic phenomena such as heterogeneous droplet sizes, drying effects, and droplet coalescence, if considered, could greatly impact granulation outcomes. For example, heterogeneous droplet sizes can lead to heterogeneous liquid distributions and ultimately a lack of granule uniformity. Likewise, effects of droplet coalescence, effective

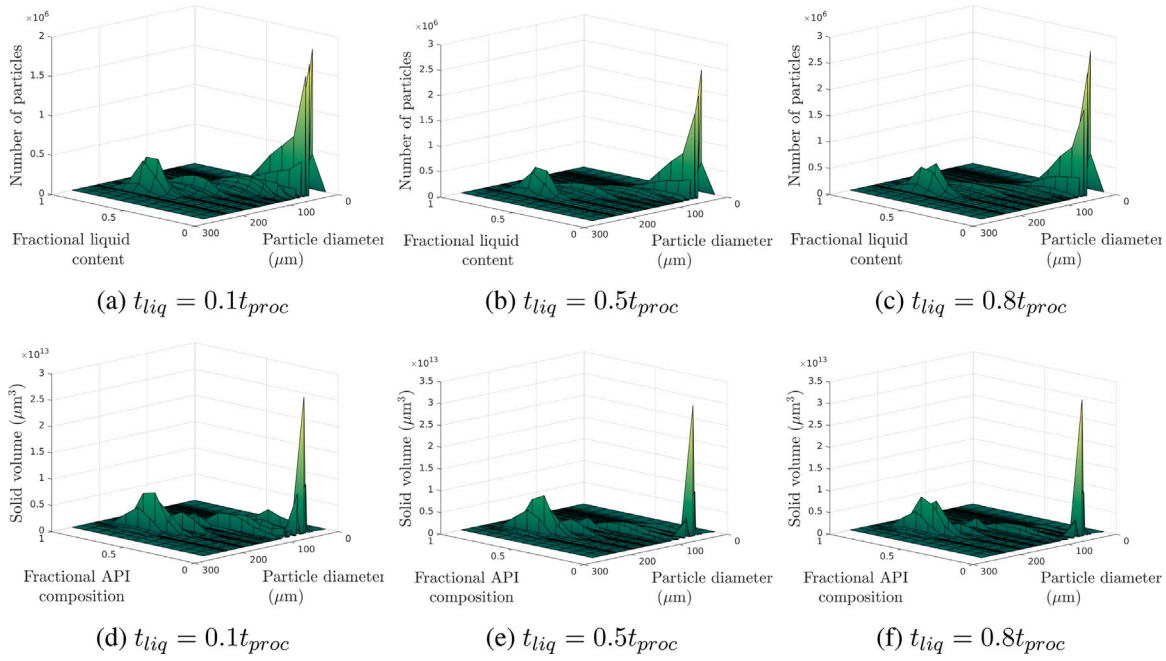

Fig. 22. The effect of different liquid addition times in the PBM-DEM coupled framework after t_{proc} = 500sec.

liquid–solid interactions in granulation may be altered. Drying effects experienced during granulation are especially important, as they have a significant impact on granule properties, including the end-state of the granule's porosity. One limitation of the current study is the use of a constant average value for the liquid absorption probability (ψ); implementing a dynamic, environment- or composition-dependent ψ could further improve mechanistic accuracy. Including all of the above phenomena in the current framework would likely require more advanced computational approaches and mathematical formulations such as CFD for drying and droplet dynamics simulations or experimental calibrations for droplet distribution and coalesce behavior. These items are interesting areas for further exploration that could make the proposed framework more relevant for practical purposes or improve overall predictive capability.

5. Conclusions

In this study, we have presented a comprehensive investigation into the development, validation, and application of a bi-directional and bi-component Population Balance Modeling-Discrete Element Method (PBM-DEM) coupling framework for simulating wet granulation processes. The proposed framework successfully couples the three-dimensional PBM with an adaptive DEM to produce accurate and efficient results. Our framework aims to accurately capture the temporal evolution of particle size, liquid, and composition distributions of a wet granulation process. Through an in-depth exploration and elaboration of the PBM, DEM, and their proposed coupling technique, we have demonstrated the framework's ability to simulate complex particulate processes efficiently.

Some of the key components introduced in the proposed framework include the dynamic Adaptive System Scaling Method (ASSM) for the DEM simulations, which adjusts the size of the simulation domain based on changes in particle sizes. Additionally, we introduced a novel liquid absorption kernel within the three-dimensional PBM setup. This kernel is represented by a mathematical approximation of liquid absorption across different particle size classes, verified through DEM simulations. The use of the liquid absorption kernel in the PBM removes the need to simulate liquid addition and absorption in every DEM coupling simulation. Hence, only the collision frequency is required in the information transfer from DEM to PBM.

The proposed framework is validated against experimental data from in the literature. The framework's versatility and accuracy in capturing the effects of process parameters on granule formation are demonstrated through two test cases, examining variations in liquid-to-solid ratio and liquid addition duration. The results confirm the framework's capability to predict the temporal evolution of particle properties, including size distribution, liquid content, and API-to-excipient mass ratio, is in agreement with experimental findings.

In conclusion, our study highlights the effectiveness of the proposed PBM-DEM coupling framework in simulating multi-component wet granulation processes. By accurately capturing the complex interplay between particle dynamics, liquid binding, and aggregation kinetics, this framework offers valuable insights for optimizing granulation processes in pharmaceutical and chemical industries. The proposed PBM-DEM coupling framework not only enhances the predictive capabilities for granulation processes but also opens avenues for further research and application in pharmaceutical manufacturing. The implications of this work are profound, promising improved efficiency and efficacy in drug formulation and production.

CRediT authorship contribution statement

Tarun De: Writing – review & editing, Writing – original draft, Software, Methodology, Investigation, Formal analysis, Data curation, Conceptualization. **Ashley Dan:** Writing – review & editing, Software, Methodology. **Rohit Ramachandran:** Writing – review & editing, Supervision, Methodology, Conceptualization. **Ashok Das:** Writing – review & editing, Writing – original draft, Validation, Supervision, Software, Project administration, Methodology, Funding acquisition, Conceptualization.

Declaration of competing interest

The authors declare that they have no known competing financial interests or personal relationships that could have appeared to influence the work reported in this paper.

Acknowledgments

The author AD acknowledges the financial support received from ANRF (PM-ECRG scheme), Govt. of India (File No.: ANRF/ECRG/

2024/006104/PMS); and FRS research grant of IIT (ISM) Dhanbad, India (Project No.: MISC 0090).

Appendix A. Supplementary data

Supplementary material related to this article can be found online at https://doi.org/10.1016/j.powtec.2025.121507.

Data availability

No data was used for the research described in the article.

References

[1] D. Barrasso, R. Ramachandran, Multi-scale modeling of granulation processes: bi-directional coupling of PBM with DEM via collision frequencies, Chem. Eng. Res. Des. 93 (2015) 304–317.

[2] C. Vervaet, J.P. Remon, Continuous granulation in the pharmaceutical industry, Chem. Eng. Sci. 60 (14) (2005) 3949–3957.

[3] A. Das, J. Kumar, M. Dosta, S. Heinrich, On the approximate solution and modeling of the kernel of nonlinear breakage population balance equation, SIAM J. Sci. Comput. 42 (6) (2020) B1570–B1598.

[4] A. Das, J. Kumar, Population balance modeling of volume and time dependent spray fluidized bed aggregation kernel using Monte Carlo simulation results, Appl. Math. Model. 92 (2021) 748–769.

[5] P.A. Cundall, O.D. Strack, A discrete numerical model for granular assemblies, Geotechnique 29 (1) (1979) 47–65.

[6] P.J. Noble, T. Weinzierl, A multiresolution discrete element method for triangulated objects with implicit time stepping, SIAM J. Sci. Comput. 44 (4) (2022) A2121–A2149.

[7] T. Tian, J. Su, J. Zhan, S. Geng, G. Xu, X. Liu, Discrete and continuum modeling of granular flow in silo discharge, Particuology 36 (2018) 127–138.

[8] G. Rozza, G. Stabile, F. Ballarin, Advanced Reduced Order Methods and Applications in Computational Fluid Dynamics, SIAM, 2022.

[9] M. Oullion, G. Reynolds, M. Hounslow, Simulating the early stage of high-shear granulation using a two-dimensional Monte-Carlo approach, Chem. Eng. Sci. 64 (4) (2009) 673–685.

[10] P. Suresh, I. Sreedhar, R. Vaidhiswaran, A. Venugopal, A comprehensive review on process and engineering aspects of pharmaceutical wet granulation, Chem. Eng. J. 328 (2017) 785–815.

[11] P. Dubovskii, V. Galkin, I. Stewart, Exact solutions for the coagulation-fragmentation equation, J. Phys. A: Math. Gen. 25 (18) (1992) 4737.

[12] V. John, T. Mitkova, M. Roland, K. Sundmacher, L. Tobiska, A. Voigt, Simulations of population balance systems with one internal coordinate using finite element methods, Chem. Eng. Sci. 64 (2009) 733–741.

[13] A. Chaudhury, A. Kapadia, A.V. Prakash, D. Barrasso, R. Ramachandran, An extended cell-average technique for a multi-dimensional population balance of granulation describing aggregation and breakage, Adv. Powder Technol. 24 (6) (2013) 962–971.

[14] R. Dürr, T. Müller, S. Duvigneau, A. Kienle, An efficient approximate moment method for multi-dimensional population balance models–Application to virus replication in multi-cellular systems, Chem. Eng. Sci. 160 (2017) 321–334.

[15] A. Das, T. De, G. Kaur, M. Dosta, S. Heinrich, J. Kumar, An efficient multi-scale bi-directional PBM-DEM coupling framework to simulate one-dimensional aggregation mechanisms, Proc. R. Soc. A 478 (2261) (2022) 20220076.

[16] A. Ding, M. Hounslow, C. Biggs, Population balance modelling of activated sludge flocculation: Investigating the size dependence of aggregation, breakage and collision efficiency, Chem. Eng. Sci. 61 (2006) 63–74.

[17] M. Hussain, J. Kumar, M. Peglow, E. Tsotsas, Modeling spray fluidized bed aggregation kinetics on the basis of Monte-Carlo simulation results, Chem. Eng. Sci. 101 (2013) 35–45.

[18] P.A. Cundall, A computer model for simulating progressive, large-scale movement in blocky rock system, in: Proceedings of the International Symposium on Rock Mechanics, vol. 8, 1971, pp. 129–136.

[19] W. Kruszelnicka, J. Diviš, J. Hlosta, Ł. Gierz, D. Žurovec, Calibration of selected bulk biomaterials parameters for DEM simulation of comminution process. Case study: corn and rice grains, Adv. Sci. Technol. Res. J. 16 (5) (2022).

[20] B. Majidi, P. Rolfe, M. Fafard, D.P. Ziegler, H. Alamdari, Numerical modeling of compaction and flow of coke/pitch mixtures using discrete element method, Constr. Build. Mater. 169 (2018) 315–324.

[21] T. De, J. Chakraborty, J. Kumar, A. Tripathi, M. Sen, W. Ketterhagen, A particle location based multi-level coarse-graining technique for Discrete Element Method (DEM) simulation, Powder Technol. (2021) 117058.

[22] J.T. Jenkins, M. Satake, Mechanics of Granular Materials: New Models and Constitutive Relations, Elsevier, 2017.

[23] A. Anand, J.S. Curtis, C.R. Wassgren, B.C. Hancock, W.R. Ketterhagen, Predicting discharge dynamics from a rectangular hopper using the discrete element method (DEM), Chem. Eng. Sci. 63 (24) (2008) 5821–5830.

[24] B. Soltanbeigi, A. Podlozhnyuk, S.-A. Papanicolopulos, C. Kloss, S. Pirker, J.Y. Ooi, DEM study of mechanical characteristics of multi-spherical and superquadric particles at micro and macro scales, Powder Technol. 329 (2018) 288–303.

[25] R. Morrison, F. Shi, R. Whyte, Modelling of incremental rock breakage by impact–for use in DEM models, Miner. Eng. 20 (3) (2007) 303–309.

[26] J.A. Gantt, I.T. Cameron, J.D. Litster, E.P. Gatzke, Determination of coalescence kernels for high-shear granulation using DEM simulations, Powder Technol. 170 (2006) 53–63.

[27] M. Dosta, T.T. Chan, Linking process-property relationships for multicomponent agglomerates using DEM-ann-PBM coupling, Powder Technol. (2022) 117156.

[28] T. De, A. Das, M. Singh, J. Kumar, Enhancing efficiency in particle aggregation simulations: Coarse-grained particle modeling in the DEM-PBM coupled framework, Comput. Methods Appl. Mech. Engrg. 417 (2023) 116436.

[29] T. Baba, H. Nakamura, H. Takimoto, S. Ohsaki, S. Watano, K. Takehara, T. Higuchi, T. Hirosawa, T. Yamamoto, DEM–PBM coupling method for the layering granulation of iron ore, Powder Technol. 378 (2021) 40–50.

[30] T. De, A. Das, J. Kumar, On the prediction of particle collision behavior in coarse-grained and resolved systems, Part. Sci. Technol. (2023) 1–15.

[31] H. Liu, M. Li, Population balance modelling and multi-stage optimal control of a pulsed spray fluidized bed granulation, Int. J. Pharm. 468 (2014) 223–233.

[32] D. Barrasso, T. Eppinger, F.E. Pereira, R. Aglave, K. Debus, S.K. Bermingham, R. Ramachandran, A multi-scale, mechanistic model of a wet granulation process using a novel bi-directional PBM–DEM coupling algorithm, Chem. Eng. Sci. 123 (2015) 500–513.

[33] M. Sen, D. Barrasso, R. Singh, R. Ramachandran, A multi-scale hybrid CFD-DEM-PBM description of a fluid-bed granulation process, Processes 2 (2014) 89–111.

[34] A. El Hagrasy, J. Hennenkamp, M. Burke, J. Cartwright, J. Litster, Twin screw wet granulation: Influence of formulation parameters on granule properties and growth behavior, Powder Technol. 238 (2013) 108–115.

[35] L. Madec, L. Falk, E. Plasari, Modelling of the agglomeration in suspension process with multidimensional kernels, Powder Technol. 130 (1–3) (2003) 147–153.

[36] A. Chaudhury, H. Wu, M. Khan, R. Ramachandran, A mechanistic population balance model for granulation processes: effect of process and formulation parameters, Chem. Eng. Sci. 107 (2014) 76–92.

[37] A. Chaturbedi, C.K. Bandi, D. Reddy, P. Pandey, A. Narang, D. Bindra, L. Tao, J. Zhao, J. Li, M. Hussain, et al., Compartment based population balance model development of a high shear wet granulation process via dry and wet binder addition, Chem. Eng. Res. Des. 123 (2017) 187–200.

[38] D. Barrasso, A. Tamrakar, R. Ramachandran, Model order reduction of a multi-scale PBM-DEM description of a wet granulation process via ANN, Procedia Eng. 102 (2015) 1295–1304.

[39] F.P. Di Maio, A. Di Renzo, Verification of scaling criteria for bubbling fluidized beds by DEM–CFD simulation, Powder Technol. 248 (2013) 161–171.

[40] L. Lu, J. Xu, W. Ge, Y. Yue, X. Liu, J. Li, EMMS-based discrete particle method (EMMS–DPM) for simulation of gas–solid flows, Chem. Eng. Sci. 120 (2014) 67–87.

[41] D. Gidaspow, Multiphase Flow and Fluidization: Continuum and Kinetic Theory Descriptions, Academic Press, 1994.

[42] C. Kloss, LIGGGHTS-PUBLIC documentation, 2016, https://www.cfdem.com/media/DEM/docu/Manual.html [Online; accessed 02-February-2019].

[43] J.M.-H. Poon, R. Ramachandran, C.F. Sanders, T. Glaser, C.D. Immanuel, F.J. Doyle III, J.D. Litster, F. Stepanek, F.-Y. Wang, I.T. Cameron, Experimental validation studies on a multi-dimensional and multi-scale population balance model of batch granulation, Chem. Eng. Sci. 64 (4) (2009) 775–786.

[44] R. Ramachandran, J.M.-H. Poon, C.F. Sanders, T. Glaser, C.D. Immanuel, F.J. Doyle III, J.D. Litster, F. Stepanek, F.-Y. Wang, I.T. Cameron, Experimental studies on distributions of granule size, binder content and porosity in batch drum granulation: Inferences on process modelling requirements and process sensitivities, Powder Technol. 188 (2) (2008) 89–101.

[45] C.C. Sun, True density of microcrystalline cellulose, J. Pharm. Sci. 94 (10) (2005) 2132–2134.

[46] S.K. Barik, C.M. Patel, V. Lad, Experimental and DEM study of flow behaviour of microcrystalline cellulose powders mix from conical silos, Mater. Res. Proc. 49 (2025).

[47] S. Oka, O. Kašpar, V. Tokárová, K. Sowrirajan, H. Wu, M. Khan, F. Muzzio, F. Štěpánek, R. Ramachandran, A quantitative study of the effect of process parameters on key granule characteristics in a high shear wet granulation process involving a two component pharmaceutical blend, Adv. Powder Technol. 26 (1) (2015) 315–322.

[48] I. Muthancheri, R. Ramachandran, Mechanistic understanding of granule growth behavior in bi-component wet granulation processes with wettability differentials, Powder Technol. 367 (2020) 841–859.